Deep learning techniques for non-destructive testing and evaluation

Roberto Miorelli, Anastassios Skarlatos, Caroline Vienne, Christophe Reboud, Pierre Calmon

Chapter 4

Deep Learning as Applied to Non-Destructive Testing and Evaluation

Roberto Miorelli[1], Anastassios Skarlatos[1], Caroline Vienne[1], Christophe Reboud[1] and Pierre Calmon[1]

4.1 Introduction

The term of Non-Destructive Testing and Evaluation (NDT&E) gathers methods and techniques aiming at assessing the material properties of media during the industrial manufacturing process (i.e., quality control, zero-defects production, etc.) of specimen and during the exploitation cycle of the manufactured specimen (i.e., integrity check, the ageing status, etc.). NDT&E is applied to test the integrity of the deployed structures in industrial domains ranging from energy (e.g., nuclear, oil&gas, power-line electric, etc.), transportation (e.g., automotive, railways, aeronautic), civil structures (e.g., bridges, buildings, etc.), manufacturing (e.g., metallurgic, food, chemical pharmaceutical, etc.) to cite the most prominent ones. The NDT&E methods are often classified by their type of energy and tha associated propagation mechanisms in the investigated specimen under testing (SUT): electromagnetic- (i.e., magnetic flux density testing, eddy current testing, microwave testing, terahertz testing), infrared (i.e., infrared thermography testing), X-rays (i.e., radiography, tomography testing) and ultrasonic- (i.e., acoustic-, elasto-dynamic, guided-wave propagation regime testing). This chapter focuses on problems dealing with electromagnetic based methods and techniques.

In the last decade, NDT&E research and development communities have been trying to develop automatic inspection systems, aiming at assisting or replacing the human involvement in data analysis and thus at enhancing productivity and reducing the risk of human errors. Indeed, in NDT&E, the measurements are normally composed of a large amount of data that can behave as (multimodal-) time-series and/or (multispectral-) images. Solutions to automatize the diagnostic process or at least to provide an assistance are currently under active research, as a consequence of the digitization of manufacturing processes, called "Industry 4.0". To this end, the NDT&E community is studying Artificial Intelligence (AI) -based approaches and machine learning (ML) -based algorithms. Among the most promising ML algorithms, the growing family of Artificial Neural Network (ANN) and in particular

[1]Université Paris-Saclay, CEA, List, F-91120, Palaiseau, France

the Deep Neural Network (DNN) -based algorithms are catching the attention of scholars and engineers (see Fig. 4.1).

Some constraints make the development and the application of ML algorithms challenging in the NDT&E context. Indeed, large collections of datasets containing close-to-reality experimental data are often not available. As a matter of fact, due to industry confidentiality constraints, collaborative and open development frameworks are quite rare and bounded on very specific cases. Another limitation is the lack of normalization of the use of such algorithms. Documents of recommended practices have been released only very recently and have not been yet applied in the various sectors of industry. The proper way of comparing performance between such solutions and actual inspection procedures still remains an open question in many sectors.

This book chapter describes the use of ML methods and techniques with a focus on DL-based methods. It provides an analysis of recent contributions within the research community. Current and future trends of the application of DL algorithms are also mentioned. Moreover, even though our analysis is based on the electromagnetic methods, we think that this contribution may partially apply to the study of other methods (i.e., ultrasound testing, structural health monitoring, acoustic emission, visual inspection etc.). Our review considers the most significant research axes in representative industrial sectors: energy, transportation, the civil engineering and manufacturing.

This chapter is organized as follows. In Section 4.2, we provide the principle of electromagnetic propagation and modelling with particular emphasis on applications in the quasi-static regime for layered homogeneous conductive media. In addition, some formal definitions about forward and inverse problems that are often recalled in the chapter are detailed. In Section 4.3, we review the main categories and challenges in applying deep learning methods to electromagnetic non-destructive testing signals analyzing the different kind of signals commonly probed by the most common electromagnetic methods and techniques. In Section 4.4, we analyze some important contributions made in the field. The analysis performed has as main purpose to shed light on the application of deep learning in the main industrial sectors concerned by electromagnetic inspection methods. In Section 4.5, we provide a brief overview of two main complementary methods for assessing the integrity of the structures. In Section 4.6, an analysis of future trends and open issues on the application of deep learning algorithms is provided. The last section is devoted to the chapter conclusion and remarks.

4.2 Principles of electromagnetic NDT&E modeling

A typical scenario for the electromagnetic inspection of a conducting and/or magnetic piece is schematically depicted in Fig. 4.3. The tested piece is interacting with an incident electromagnetic field produced by a set of inducting coils, and the resulting field is sensed via a number of probes scanning the piece at the region of interest. The detection probe can be either an induction coil (with or without ferrite core), which can be designed to adapt to the specific geometrical features of the piece

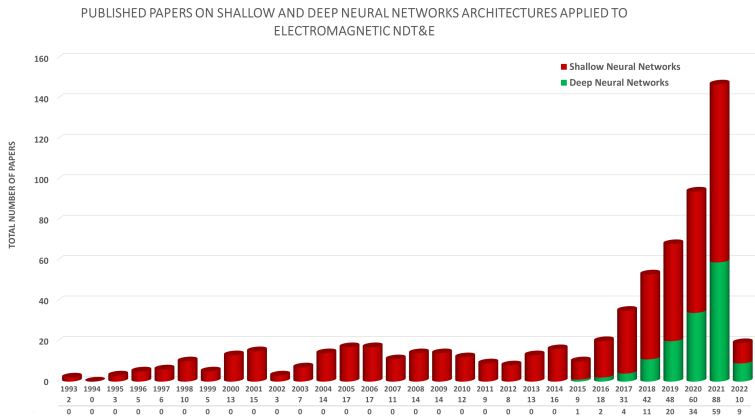

Figure 4.1 Estimated number of papers applying deep and shallow neural networks methods to electromagnetic NDT&E problems (Source:Web Of Science, data updated to February 2022).

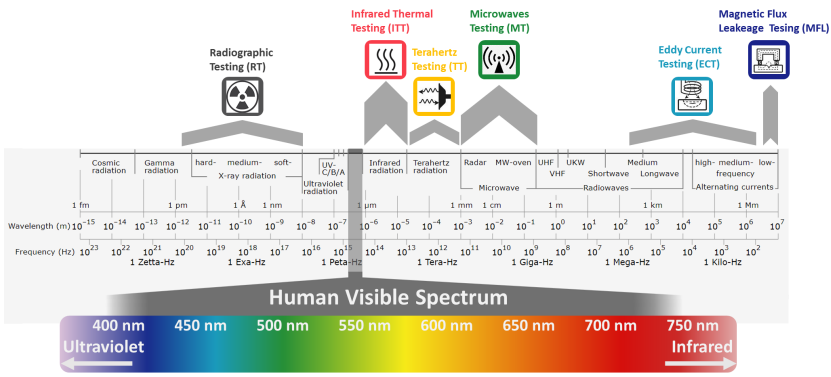

Figure 4.2 NDT&E methods as localized on the electromagnetic spectrum.

[1] or a magnetic field sensor, like a Hall-effect probe, a Giant Magneto-Resistance (GMR) sensor or a flux-gate, to mention the most popular ones. The measured signal carries information about the geometry and the material of the piece and it is the so-called "measurement" that will be used in the inversion phase to retrieve information about the piece.

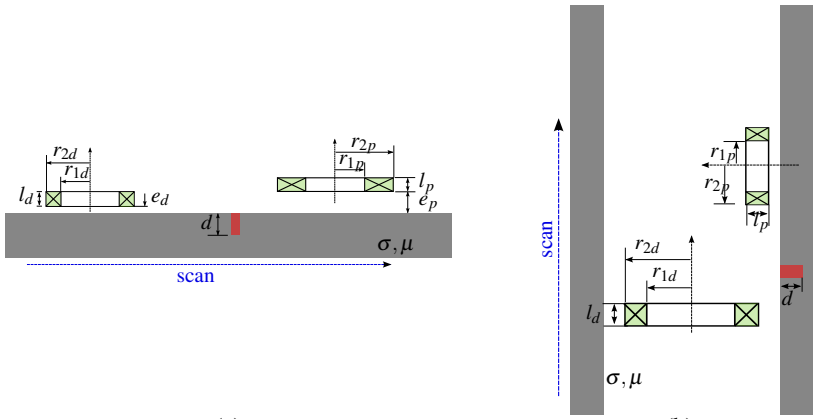

Figure 4.3 Electromagnetic inspection of (a) planar piece, (b) tube, in driver-pickup mode. One can distinguish the piece, the driver (d) and pick-up (p) coils and the defect (in red). The eddy-current head comprising the coils is scanning the piece along the dashed line.

To remain simple with the problem formulation, we shall restrict ourselves in the context of this article with inspection in the harmonic regime, which is the most wide-spread, i.e. a harmonic time dependence of the $e^{j\omega t}$, with ω being the angular frequency and $j = \sqrt{-1}$, will be assumed from this point forward for all state variables. Transient signals measurements are also used for particular applications [2, 3, 4, 5, 6, 7, 8, 9].

It is convenient for both the mathematical analysis and signal interpretation purposes to decompose the measured signal into a sum of contributions, each one expressing a particular effect. Hence, the complete signal is composed of the probe response in air, the variation owing to the presence of the piece nearby the probe and finally the small signal variation sensed when scanning a flawed area of the piece. As these contributions have very different amplitudes and spatial properties, it is often much more efficient to compute them separately using perturbation approaches.

In case of Fig. 4.3 (single receiving coil), the measurement signal is proportional to the mutual impedance ΔZ_{TR}, where T stands for "transmitter" and R for receiver. The total impedance can be split in three parts, namely the mutual impedance in air $\Delta Z_{TR}^{(a)}$, the impedance change due to the piece $\Delta Z_{TR}^{(p)}$, referred to usually as the "ge-

ometry signal" and finally the impedance change owing to the presence of material defects in the illuminated zone $\Delta Z_{TR}^{(p)}$. One can thus write

$$\Delta Z_{TR}(\mathbf{r}_s, \omega) = j\omega M_{TR}^{(a)} + \Delta Z_{TR}^{(p)}(\mathbf{r}_s, \omega) + \Delta Z_{TR}^{(d)}(\mathbf{r}_s, \omega) \tag{4.1}$$

where $M_{TR}^{(a)}$ is the mutual inductance in air. Notice that both the geometry and the defect signals depend on the probe position $\mathbf{r}_s$. In the case of a magnetic field sensor, the previous splitting of the total signal in air, piece and defect contributions also holds, where this time the complex impedance should be replaced by the magnetic field component parallel to the sensitivity direction of the magnetic sensor. In the following, we shall focus on the former case, since coils are the preferred probes in the majority of practical applications. The analysis is similar for magnetic field measurements.

From the three parts in (4.1), $M_{TR}^{(a)}$ only depends upon the probe geometry and does not carry any information on the piece. It is therefore not useful for the purposes of signal processing. Besides, being constant for all scan positions, it can be easily removed by calibration. Our primary concern will thus be the calculation of the remaining two terms, namely the geometry and the defect perturbation signals.

4.2.1 Field solution for the flawless piece and calculation of the signal geometry $\Delta Z_{TR}^{(p)}$

Referring to the above introduced air-piece-defect decomposition approach, the next step in the analysis will be to calculate the response of the flawless piece, i.e. the scattering field and the probe signal owing to the piece interaction with the coil field.

The treatment of the geometry signal $\Delta Z_{TR}^{(p)}$ can provide information about the piece material and global configuration parameters such as the piece thickness, the probe lift-off, etc. Since it depends only upon the geometry of the flawless piece, it can be often calculated by semi-analytical approaches. There is a large number of articles concerned with this calculation, all stemming in a greater of lesser extent on the seminal work of Dodd and Deeds in the 60s [10, 11] and the Auld's article on the specialization of the Lorentz reciprocity theorem [12, 13]. This approach has been greatly enhanced and extended by Theodouldis and Bowler with the introduction of the Truncated Region Eigenfunctions Expansion (TREE) [14, 15, 16, 17]. The TREE method has thus permitted the calculation of the geometry signal for canonical pieces with discontinuities like edges [18] boreholes [19, 20, 21, 22], tubes with eccentric walls [23] etc. For more complicated pieces one has to resort to either fully numerically techniques like the Finite Element Method (FEM) or hybrid analytical-numerical schemes [24].

In the case of a symmetric piece, the signal geometry is also constant, and can be thus separated from the flaw signal by a simple-baseline removal.

4.2.2 Defect response: calculation of the flaw signal $\Delta Z_{TR}^{(d)}$

We assume that the flawless piece is homogeneous and isotropic in the region of interest with a "base" electrical conductivity σ_b and magnetic permeability μ_b. The presence of material defects is translated to a local variation of the piece electric and magnetic properties, $\delta\sigma(\mathbf{r})$ and $\delta\mu(\mathbf{r})$, respectively. The material coefficients in the piece with the flaw can be thus written in the following way

$$\sigma(\mathbf{r}) = \sigma_b + \delta\sigma(\mathbf{r}) \tag{4.2}$$

$$\mu(\mathbf{r}) = \mu_b + \delta\mu(\mathbf{r})\,. \tag{4.3}$$

The interaction of the driving (primary) electric and magnetic field $\mathbf{E}_p, \mathbf{H}_p$ with the material inhomogeneities owing to the flaw, can be seen as the effect of an equivalent electric and an equivalent magnetic source, which superposed to $\mathbf{E}_p, \mathbf{H}_p$ will yield the total field according the expressions [25, 26, 27, 28, 29]

$$\begin{aligned}\mathbf{E}(\mathbf{r}) = \mathbf{E}^p(\mathbf{r}) &- j\omega\mu_b \int_{V_f} \overline{\mathbf{G}}^{ee}(\mathbf{r},\mathbf{r}') \cdot \delta\sigma(\mathbf{r}')\,\mathbf{E}(\mathbf{r})\,dV' \\ &- j\omega \int_{V_f} \overline{\mathbf{G}}^{em}(\mathbf{r},\mathbf{r}') \cdot \delta\mu(\mathbf{r}')\,\mathbf{H}(\mathbf{r}')\,dV'\end{aligned} \tag{4.4}$$

$$\begin{aligned}\mathbf{H}(\mathbf{r}) = \mathbf{H}^p(\mathbf{r}) &+ \int_{V_f} \overline{\mathbf{G}}^{me}(\mathbf{r},\mathbf{r}') \cdot \delta\sigma(\mathbf{r}')\,\mathbf{E}(\mathbf{r}')\,dV' \\ &- j\omega\sigma_b \int_{V_f} \overline{\mathbf{G}}^{mm}(\mathbf{r},\mathbf{r}') \cdot \delta\mu_b(\mathbf{r}')\,\mathbf{H}(\mathbf{r}')\,dV'.\end{aligned} \tag{4.5}$$

where $\overline{\mathbf{G}}^{ee}$, $\overline{\mathbf{G}}^{me}$, $\overline{\mathbf{G}}^{em}$, $\overline{\mathbf{G}}^{mm}$ stand for the Green's dyads of the host medium. The integration is carried out over the defect(s) support V_f.

The $\overline{\mathbf{G}}^{ee}$ and $\overline{\mathbf{G}}^{me}$ dyads are defined as the electric and magnetic field response with a unit Dirac electric current source satisfying the Helmholtz equation [25, 29]

$$\nabla\times\nabla\times\overline{\mathbf{G}}^{ee}(\mathbf{r},\mathbf{r}') + j\omega\mu\sigma\overline{\mathbf{G}}^{ee}(\mathbf{r},\mathbf{r}') = \bar{\mathbf{I}}\delta(\mathbf{r}-\mathbf{r}') \tag{4.6}$$

$$\nabla\times\nabla\times\overline{\mathbf{G}}^{me}(\mathbf{r},\mathbf{r}') + j\omega\mu\sigma\overline{\mathbf{G}}^{me}(\mathbf{r},\mathbf{r}') = \nabla\times\left[\bar{\mathbf{I}}\delta(\mathbf{r}-\mathbf{r}')\right] \tag{4.7}$$

where $\delta(\mathbf{r}-\mathbf{r}')$ is the delta function, and $\bar{\mathbf{I}}$ stands for the unit tensor. $\overline{\mathbf{G}}^{mm}$ and $\overline{\mathbf{G}}^{em}$ are defined in a similar way, as the corresponding magnetic and electric field response under magnetic current excitation, and they satisfy the same equations (4.6) and (4.7), respectively.

Note that the two pairs are interrelated via the duality principle, i.e., they can be interchanged in (4.6) and (4.7) using the following rule $\overline{\mathbf{G}}^{ee} \leftrightarrow \overline{\mathbf{G}}^{mm}$ and $\overline{\mathbf{G}}^{me} \leftrightarrow \overline{\mathbf{G}}^{em}$, which together with the interchanges $\mathbf{E} \leftrightarrow \mathbf{H}$, $\sigma \leftrightarrow -j\omega\mu$ produce the same set of equations. The duality transformation constitutes hence a symmetry of (4.6) and (4.7). The detailed derivation of the Green's dyads in planar and cylindrical stratified media is given in [25, 29].

The mutual impedance variation owing to the flaw is calculated using the above solution in an elegant way by application of the reciprocity theorem

$$\Delta Z_{TR}^{(d)}(\mathbf{r}_s) = -\frac{1}{I_T I_R}\int\limits_{V_f} \big[\delta\sigma(\mathbf{r}')\,\mathbf{E}_T(\mathbf{r}';\mathbf{r}_s)\cdot\mathbf{E}_R^p(\mathbf{r}';\mathbf{r}_s) - j\omega\delta\mu(\mathbf{r}')\,\mathbf{H}_T(\mathbf{r}';\mathbf{r}_s)\cdot\mathbf{H}_R^p(\mathbf{r}';\mathbf{r}_s)\big]\,dV' \tag{4.8}$$

where $\mathbf{E}_R^p$ and $\mathbf{H}_R^p$ stand for the electric and magnetic field in the flawless medium that would be produced is the receiver coil would be fed with current I_R. $\mathbf{E}_T, \mathbf{H}_T$ is the field solution obtained by (4.6) and (4.7) with the transmitting coil being active and fed with current I_T. Notice the functional dependence of the field terms from the probe position $\mathbf{r}_s$ denoting that one has to consider a different field solution per scan point. The angular frequency dependence of all variables is implied.

In case of direct magnetic field observations, (4.8) should be replaced by a calculation of the magnetic field at the probe position, namely (4.7) using the suitable expressions for the Green's dyads $\overline{\mathbf{G}}^{em}$ and $\overline{\mathbf{G}}^{mm}$[2].

Conductive, non-magnetic medium with volumetric flaws

Eqs. (4.4)-(4.8) address the most general case of a defect inside a conducting and magnetic medium. However, in practical applications this general case concerns only ferritic steels since steel is the only ferromagnetic material of industrial interest. For the rest of workpieces the magnetic contribution due to the permeability difference is negligible, i.e., $\delta\mu = 0$ and (4.4)-(4.8) specialize to the following relations for the state equation

$$\mathbf{E}(\mathbf{r}) = \mathbf{E}^p(\mathbf{r}) - j\omega\mu_b\int\limits_{V_f}\overline{\mathbf{G}}^{ee}(\mathbf{r},\mathbf{r}')\cdot\delta\sigma(\mathbf{r}')\,\mathbf{E}(\mathbf{r}')\,dV' \tag{4.9}$$

and the reciprocity theorem

$$\Delta Z_{TR}^{(d)}(\mathbf{r}_s) = -\frac{1}{I_T I_R}\int\limits_{V_f}\delta\sigma(\mathbf{r}')\,\mathbf{E}_R^p(\mathbf{r}';\mathbf{r}_s)\cdot\mathbf{E}_T(\mathbf{r}';\mathbf{r}_s)\,dV'. \tag{4.10}$$

Magnetic medium with volumetric flaws

This case concerns magnetic pieces with a local variation of the permeability value, the same time that its conductivity remains constant (i.e. $\delta\sigma = 0, \delta\mu \neq 0$, and the problem reduces to (4.5) with solely magnetic contributions. Practically this case is met in the inspection of ferromagnetic specimens using static magnetic fields, a technique known as Magnetic Flux Leakage (MFL). Since $\omega \to 0$ in this limiting case (4.5) does not provide an adequate description any more. Indeed (4.5) is derived using the Faraday induction law. To address the static problem one must devise an alternative integral equation derived by the magnetostatic equations.

[2]For a multilayer medium, like the ones considered in this class of problems, the Green's dyads expressions are different when source $\mathbf{r}'$ and $\mathbf{r}$ are located in different layers. This is the case for the observation equation, where the source (defect) lies in the medium whereas the observation is carried out in the air.

A similar problem arises when calculating the magnetic flux concentration in inductors with ferrite cores. This time is the base conductivity that goes to zero $\sigma_b \to 0$ since ferrites are electrical insulators, and the integral term in (4.5) vanishes requiring again special formulation valid for the magnetostatic regime. A treatment of the core problem using a dedicated integral equation formalism can be found in [27]. The case of a pure magnetic flaw will not be examined any further.

Conductive, non-magnetic medium with thin flaws

In non-magnetic media, a further simplification is also possible, when the thickness of the defect is negligible with respect to the other dimensions and with respect to the skin-depth in the material. This is the case of thin cracks, which is a very common category of material defects comprising the Stress-Corrosion Cracking (SCC) and the Fatigue Crack (FC) mechanisms. The appropriate formalism for the modelling of cracks in infinite medium has been introduced by Bowler *et al.* [30, 31, 32, 33, 34] and has been extended in the recent literature by Theodoulidis and Miorelli *et al.* [35, 36, 37]. Further developments have addressed the cases of finite media accounting end-effect such as plate edges by Theodoulidis and Bowler [38], boreholes by Pipis *et al.*, Skarlatos and Theodoulidis [22, 39] and tube edges [40].

Using the fact that the normal current component at the surface of the crack must vanish, which in its turn is translated to vanishing normal electric field, (4.9) reduces to

$$\mathbf{n}\cdot\mathbf{E}^p(\mathbf{r}) = j\omega\mu_b \int_{S_f} \mathbf{n}\cdot\overline{\mathbf{G}}^{ee}(\mathbf{r},\mathbf{r}')\cdot\mathbf{n}\; p(\mathbf{r}')\, dS' \tag{4.11}$$

where S_f is the crack surface and p expresses the electric dipole distribution over S_f, defined as

$$p(\mathbf{r}) = \lim_{\Delta x\to 0} \delta\sigma(\mathbf{r})\,\mathbf{n}\cdot\mathbf{E}(\mathbf{r})\,\Delta x \tag{4.12}$$

with Δx the crack opening and $\mathbf{n}$ the unit normal to S_f.

Notice the simplification achieved when moving from (4.9), which is a vector Fredholm integral equation of the second kind, with (4.11), a first order scalar Fredholm equation. The reciprocity relation is also simplified accordingly

$$\Delta Z_{TR}^{(d)}(\mathbf{r}_s) = -\frac{1}{I_T I_R}\int_{S_f} \mathbf{n}\cdot\mathbf{E}_R^p(\mathbf{r}';\mathbf{r}_s)\; p_T(\mathbf{r}';\mathbf{r}_s)\, dS'. \tag{4.13}$$

The interpretation of the T, R indices remains the same as above.

4.2.3 Examples

The application of the integral method approach for the calculation of the defect response will be illustrated via two examples.

The first example deals with the signature of a circumferential defect in a ferromagnetic tube obtained using a Remote-Field Eddy-Current (RFEC) probe. The problem configuration is depicted in Fig. 4.4a.

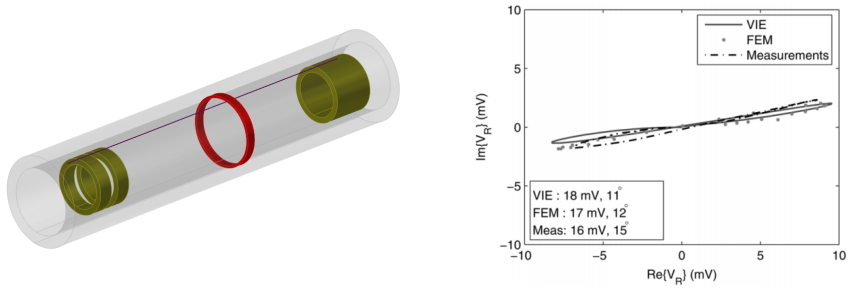

(a) (b)

Figure 4.4 Eddy-current inspection of a ferromagnetic tube using a REFC probe. (a) Piece geometry and probe. The red ring stands for the defect. (b) Comparison of the simulation results obtained using the integral method approach and the FEM method with measurements (experimental data courtesy of Chen et al. [41, 42]) (Copyright IEEE).

The probe consists of a 15 mm long transmitting coil and an axial gradiometer with two coils connected in differential mode. Both receiving coils have 5 mm thickness and are located in the remote field region. The considered defect is a 50% thick (percentage with respect to the tube wall) and 5 mm wide inner groove. The results of the integral method presented above are compared against FEM simulations and measurements in Fig. 4.4. The illustrated curves stand for the complex plane representation of the gradiometer signal as function of the probe position. This is a very common representation in Eddy Current Testing (ECT) applications since the form and the angle of the curves provide direct information about the defect features.

The second example concerns a fastener inspection affected by a narrow crack. This is a application in the aeronautical industry, namely the eddy-current testing of fuselage fasteners. Notice that the riveted structures are regions prone to the appearance of cracks owing to mechanical stress concentrations there. The considered set-up is shown in

In this specific configuration, the fastener hole can be either considered as a large defect which is addressed by means of the integral equation (4.9), a solution proposed in [43], or alternatively as integrated part of the geometry, in which case one needs to construct the appropriate Green's dyad that takes into account all interfaces of the piece (horizontal interfaces and hole surface) as done in [39]. In the former case, the Green's dyad calculation is more straightforward, however the discretisation of the defect has a negative impact to the computational burden. The latter approach is computationally more efficient, yet one has to cope with the construction of the appropriate Green's function, which is a hard problem.

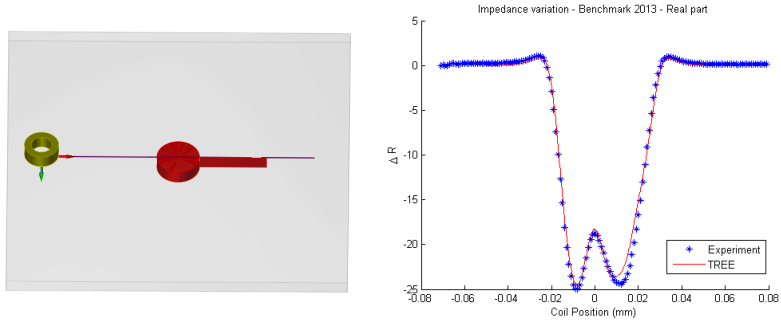

(a) (b)

Figure 4.5 ECT of fastener with a narrow crack. (a) Problem geometry. (b) Simulation vs experimental results (real part). The signal asymmetry is due to the presence of the crack (Copyright IEEE).

4.2.4 *Inverse problems by means of optimization and machine learning approaches*

In the previous sections we provided an overview of some computational methods that can be used to address the direct problem, that is to calculate the probe response for a given configuration of inspection. This *forward model* will from now on correspond to a function $f(\mathbf{x}|\mathbf{r}_s)$ that calculates the measured signals with respect to the probe position $\mathbf{r}_s$, with $\mathbf{x}$ being some set of parameters representing the features of the geometry which we wish to estimate (conductivity, permeability, crack dimensions, crack position, etc.).

In a typical optimization approach, the forward model f is evaluated in a loop and compared with measurements $\mathbf{y}$ to recover an estimate of $\mathbf{x}$ by solving a minimization problem [44],

$$f_{obj}^{-1} := \underset{x}{\operatorname{argmax}}\, mis\left\{f(\mathbf{x}|\mathbf{r}_s), \mathbf{y}\right\} + R(\mathbf{x}) \tag{4.14}$$

where mis: $Y \times Y \rightarrow R^+$ is an appropriate measure of discrepancy in the data domain, and $R : X \rightarrow R^+$ is a regularization functional that incorporates our prior knowledge of $\mathbf{x}$. For a nonlinear inverse problem, (4.14) is usually solved by iterative methods, and in some cases it can be converted to an approximate direct inversion model. The minimizer of (4.14) is the solution provided by the objective function approach. Some typical implementations of the misfit function comprise the L^2 norm of the (normalised) difference between simulated and measured data or some kind of energy functional.

Alternatively, machine learning algorithms can be used for solving inverse problems in NDT&E. The learning approach consists first in collecting a sufficiently large amount of measured data $\mathbf{y}$, or synthetic data $f(\mathbf{x}|\mathbf{r}_s)$ and the corresponding values of parameters $\mathbf{x}$, forming a so-called training set of N pairs $\{(x_n, y_n)\}$, $n = 1, \ldots, N$. This training set is then used to fit a ML model $\mathscr{F}_\theta(\mathbf{y})$ able to estimate $\mathbf{x}$, with $\theta \in \Theta$ the specific parameters of the ML model. In case of deep learning methods, $\mathscr{F}_\theta(\mathbf{y})$

corresponds to the architecture employed for solving the problem parametrized by $\theta \in \Theta$. The deep learning architectures parameters are fitted to the training set during the so-called training phase (or stage) that is performed off-line by solving the optimization problems [44]

$$f^{-1}(\mathbf{y}) := \mathscr{F}_{\theta}(\mathbf{y}), with\, \theta\, being \underset{\theta \in \Theta}{\operatorname{argmin}} \sum_{n=1}^{N} mis\{\mathscr{F}_{\theta}(\mathbf{y}_n), \mathbf{x}_n\} + R(\theta) \quad (4.15)$$

where *mis*: $X \times X \rightarrow R^{+}$ is a suitable measure of the mismatch in the parameter space and $R : \Theta \rightarrow R^{+}$ is used to regularize the solution and enhance the model generalization capabilities (i.e., avoid overfitting). Different metrics can be used to assess model mismatch depending on the learning task objective (e.g., classification or regression tasks) and the architecture employed [45]. The minimization of (4.15) is obtained through back-propagation algorithms by using a broad set of efficient minimizers (e.g., Adam, AdaGrad, RMSProp, SGD) [45]. Therefore, prediction (also called test phase) can be performed in almost real time just by evaluation of the model on an unknown set of measurements $\mathbf{y}_{test}$ such that $\hat{\mathbf{x}}_{test} = \mathscr{F}_{\theta}(\mathbf{y}_{test})$. It is worth mentioning that deep learning approaches can also be used to perform forward modelling tasks: in this case the model learns to generate signals $\mathbf{y}$ from a set of parameters $\mathbf{x}$.

4.3 Applications of deep learning approaches for forward and inverse problems in NDT&E

In NdT&E research and development community, numerical simulations have been historically used to design probes, inspection set-ups and assess inspection performance minimizing as much as possible time-consuming and expensive experiments. More recently, simulations have been widely exploited in order to carry out very computational demanding calculations involving statistical and sensitivity analysis studies. In this framework, ML algorithms have been employed in order to build surrogate models (also called metamodels) to speed-up otherwise computationally infeasible studies. NDT&E scholars refer to such ML paradigm as model- or physics-driven approach in contrast to the data-driven approach where ML algorithms are fit directly to measured data.

In NDT&E, model-driven ML approaches exploit the knowledge on the problem coming from simulations in order to design a suitable numerical experiment to be used for training supervised classification and regression algorithms. Once the algorithm is trained, then its performance is evaluated on a meaningful test set. Depending on the situation, the test set can be purely numerical, experimental or a mix of the two. The performance of such a ML schema on the experimental test set can be affected by the level of agreement between experimental acquisitions and simulated data. Such an agreement depends on two main uncertainty factors, the epistemic and the aleatoric uncertainties [46, 47]. The epistemic uncertainty factor can be reduced by designing a suitable ML schema or by increasing the number of simulated samples. The aleatoric uncertainty cannot be reduced since it is intrinsic to the experimental set-up. Common sources of aleatoric uncertainty, one can mention

experimental noise, probe ageing and misplacement, lack of knowledge on specimen characteristics and defect(s) morphology, etc. These uncertainties may greatly impact the ability of a trained ML model to be applied to real experimental data.

Data-driven approaches are widely employed by ML signal and image processing communities as it has access to large of real (e.g., recorded audio signals, images, etc.) open access datasets counting, very often, more than hundred of thousand of samples. Unfortunately, in developing model-based ML strategies tackling NDT&E inspection problems for forward and inverse tasks, one needs to face two main issues. First, very few open access experimental datasets are available, thus it is difficult to establish common benchmarks to test and improve the state-of-the-art of ML-based strategies developed. Secondly, probed data are very often inspection and case dependent. Indeed, even in a pure data-driven approach, the aleatoric uncertainties on a given inspection problem may lead to poor generalization capabilities of the ML algorithms developed on unseen test samples (i.e., same inspection problem but an unseen experimental set-ups). Furthermore, in NDT&E acquisitions, the large majority of probed signals and/or images concerns healthy specimens, whereas to detect flaws one need to have a lot of signals coming from flawed specimen to learn from. In classification tasks, imbalanced datasets between healthy and unhealthy specimens or between falw types is very common and must be properly handled in the training phase. In addition, training data are often partially labelled or not at all labelled, which means that signals are available but not the corresponding information (we have the $\mathbf{y}$ data but not the corresponding values of $\mathbf{x}$ like the probe(s) position, the defect(s) geometry, the specimen characteristics, etc..). This limits the options of algorithms to so-called semi-supervised ones, which have lower performance than their supervised counterparts.

The NDT&E research community has attempted to mitigate the drawbacks associated to model-driven and data-driven ML schema by adopting different strategies. The NDT&E researchers have tried to inject physics-based knowledge in order to tailor a specific ML schema. Toward this end, specific features engineering techniques have been applied on probed signals in order to promote descriptors minimizing the aleatoric uncertainty contribution and thus enhancing the ML model generalizations performance. Furthermore, the joint use of synthetic data (which are cheaper to generate and are always labelled) and experimental data (which are similar to the test data that will be used in the end) in training sets is currently a hot research topic.

In electromagnetic NDT&E one can distinguish two main categories of probed data. The first category gathers signals that behave like time-series signals such as scanning signal with respect to probe(s) displacement (e.g., eddy current testing acquisitions in 2D symmetrical problems) or time (e.g., pulsed eddy current testing signals for a given probe position). The second category collects all signals that can be seen as 2D cartographies (e.g., eddy current testing acquisitions in 3D problems) or 1D probe(s) displacement and a succession of time steps (e.g. a pulsed eddy current acquisition). For both categories, very often, probed signals are complex-valued and both real and imaginary parts are analyzed since the informative contents. Furthermore, multi-static probe arrays and multi-frequency acquisitions have to be considered to fulfill the inspection protocols, so the images analysed can be seen as

multi-spectral ones. That is, typical electromagnetic NDT&E acquired signals behave as tensors with typical orders between 2 to 4. It is worth to be mentioned that, thanks to the high flexibility in designing DL architecture, different source and/or different extractions (also called ways in the signal processing community) of the same data can be merged, mixed or exploited smoothly, making the use of DL methods a very convenient and flexible tool for features extraction and fusion in NDT&E.

4.3.1 Most relevant deep learning architecture in NDT&E

A deep learning architecture [45] consists in a chain of mathematical operations established between inputs and outputs, the so-called layers. That is, the layers perform transformation on inputs in order to extract the most meaningful features to perform the final tasks (e.g., regression, classification, etc.). Each layer is composed by arithmetic units, called neurons, that enable the mathematical transformations. In the most common deep learning architecture, the output of one layer is fed to the the next layer neuron through a linear combination of weights and biases θ (i.e., see (4.15)). On these linear operations is applied an element-by-element non-linear transformation through the use the so called activation functions (or layer) aiming at handling non-linear behaviour in mapping two successive layers. The most common activation functions are the sigmoid, Rectified Linear Unit (ReLu), Leaky-ReLU, softmax, etc. The use of a particular activation function depends on the task associated to the layer to which it is attached.

From a general point of view, the connections between two layers identifies the architecture type, e.g., Fully Connected Neural Network (FCNN), Multi-Layer Perceptron (MLP), Convolutional Neural Network (CNN), Long Short Time Memory Recurrent Neural Network (LSTM- RNN) just to cite the most prominent ones. Furthermore, provided a given family of layers (e.g., CNN, FCNN, etc.), different architectures topologies (e.g., encoder-decoder, U-Net, etc.) can be obtained by connecting the different layers together in order to solve the problem at the hand. Furthermore, the deep learning architecture can be also classified with respect to the machine learning task to be handled. That is, one can divide the architectures by considering supervised, semi-supervised and unsupervised learning paradigms. The most used DL architectures that we will study in this chapter belong to the supervised learning framework aiming at solving regression and classification tasks based on labelled datasets. Nevertheless, unsupervised learning (i.e., no labels are attached to the data) based on the use of use generative models such as Variational AutoEncoder (VAE), Generative Adversarial Network (GAN), etc. is becoming more and more common to solve specific tasks in the NDT&E research community. The semi-supervised learning approach is also studied to enhance the DL model accuracy when a small amount of labeled data is available.

4.4 Application of deep learning to electromagnetic NDT&E

One of the first attempts in using machine learning algorithms based on the shallow neural network in the context of eddy current testing can be goes back to the mid-

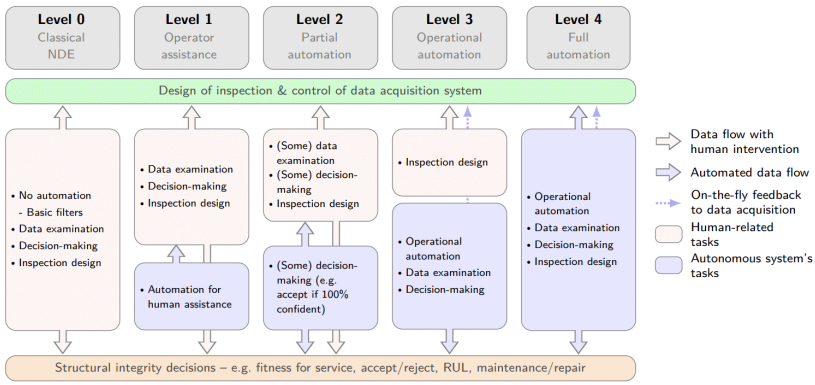

Figure 4.6 Flow chart describing the integration between human and machine learning based algorithms in performing decisions and tasks in NDT&E [65] (CC BY 4.0 license).

dle of the nineties [48, 49, 50, 51, 52, 53, 54, 55, 56]. Meanwhile, researchers in NDT&E studied the use of kernel machines such as support vector machines, kernel ridge regression, Gaussian process regression, etc., algorithms along with the use of feature extraction and feature selection techniques such as principal component analysis, partial least square, locally-linear embedding, etc. [57, 58, 59, 60, 61]. More recently, pushed by the large leap forward in performance of deep learning methods obtained in image and signal processing, the NDT&E community is actively developing and adapting deep learning architectures to handle classification and regression problems based on NDT&E inspected signals (see Fig. 4.1).

The actual research of ML tools applied to electromagnetic NDT&E is trying to propose solid and reliable solutions to support and automatize the decision processes (i.e., defect(s) detection, localization, sizing, remaining useful life (RUL), etc.) during acquisitions. In NDT&E, different levels of automation are envisaged. The integration of decisions between human supervision and machine learning algorithms is performed based on different contributions on the final outcomes. Referring to [62, 63, 64, 65], the automation levels of NDT&E inspection systems can be divided into five levels where the increasing contribution of ML algorithms impact the final decision ranging from a mild NDT&E operator assistance to a fully automatic system (see Fig. 4.6). The higher the level the most involved and complex the ML algorithms are. The complexity of the algorithm developed should also be accounted for, in view of deploying the algorithms on embedded measurements systems that need to fulfill CPU efficiency constraint and traceability of the deployed algorithm, too. In the following, we provide a systematic analysis of deep learning methods applied to industrial sectors where electromagnetic-based NDT&E is widely employed.

4.4.1 Deep learning in electromagnetic NDT&E applied to the energy sector

The energy sector gathers a very broad set of industrial sectors ranging from the nuclear energy to the renewable energies (e.g., eolian, solar, etc.) and the oil&gas. For all these industrial sectors, electromagnetic NDT&E is widely employed. In nuclear industry periodic inspection of Nuclear Power Plants (NPP) Steam Generation Tubes (SGTs) is carried out with eddy current testing methods, by means of different probe(s) arrangements and inspection protocols depending on the inspected part under test (e.g., U-bended SGT part, straight part, transition zone, near support plate, etc.). The use of AI and ML based analysis of inspection data is actually a very active research topic in order to speed-up the analysis of the very large quantity data acquired (e.g., a typical NPP is composed of hundreds of SGTs). The perspective, in the near future, of deployment of new array probes for these applications will increase considerably the amount of data to be analyzed, forcing the current organization, partly or exclusively based on manual analysis by experts, to adapt. This makes this topic quite strategic. In this context, the development of support tools for helping NDT&E engineers decisions are under study for reducing as much as possible the human analyses errors (e.g., the so-called human factor) when repetitive and long analysis are performed.

The use of deep convolutional neural network for defect detection has been proposed by Zhu *et al.* [66] based on multi-frequency ECT acquisitions performed in SGT. The data-driven schema developed involves the use of robust principal component analysis to properly detect the regions of interest. Thus, the Convolutional Neural Network (CNN) model proposed computes both the probability associated to the tested samples along with the epistemic uncertainty associated to the detected class (see Fig. 4.7). Such an approach is supposed to be widely exploited by the NDT&E community in the near future along with the possibility to embed the explainability of a deep learning method. In [67], the authors studied the performance of a deep neural network for defect classification based on the use of two different ECT probes (i.e., pancake coil and +Point probe) signals. The analysis performed showed that the neural network schema adopted was able to classify, with good performance, the longitudinal, circumferential and no-defect classes. Li *et al.* [68] proposed a first attempt to crack profile reconstruction based on the use of multi-frequency ECT signals. In particular, a C-scan ECT signal was used as input to a tailored the encoder-decoder deep neural network developed for this purpose loosely inspired by deep convolutional generative adversarial network architectures developed by the image and signal processing communities. The results obtained, based on numerical datasets only were quite promising in view of an extension to more challenging problems, e.g., involving experimental signals. In [69], a set of deep residual convolutional neural networks has been tested for crack depth classification based on massive set of acquisitions performed on steel plate containing 20 machined slot defects. The study showed that the architectures considered were capable to distinguish the different defects classes with good accuracy.

In Oil and Gas (O&G) and petrochemical industries, the use of ECT method, based on both time-harmonic excitation and Pulsed Eddy Current Testing (PECT), is

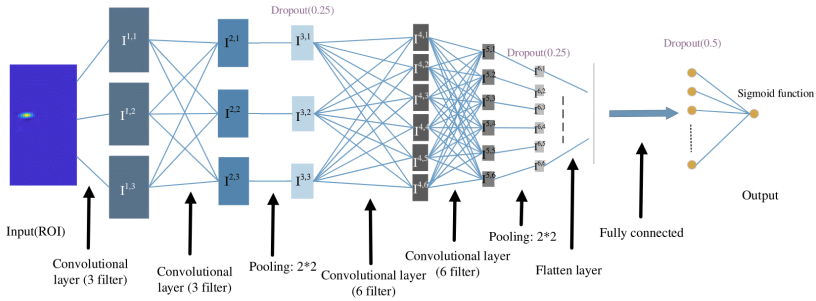

Figure 4.7 Deep convolutional neural network architecture for defect detection in SGT tube based on ECT signals enabling prediction uncertainty estimations [66] (Copyright Elsevier).

widely used for inspecting the presence of corrosion in pipelines. Detection, localization and sizing (mainly in term of corrosion thickness) are the main outcomes expected by the analysis of the data acquired. The use of machine learning algorithms is expected to provide many advantages in data analysis. For instance, in PECT the interaction of a broadband signal (e.g., pulse wave form) with the SUT produces specific signatures in time and space (i.e., probe position). Unlike more common time-harmonic excitation ECT, the analysis of PECT signals needs to account for the time dimension since a certain amount of information (e.g., material characteristics, defect properties, etc.) is embedded in the SUT feedback when the PECT excitation decay. However, a time dimension composed of hundred or even thousand of samples adds to 2D mechanical scan, making the problem computationally more demanding from the learning perspective. In order to efficiently handle such large size of data, a feature extraction of probed signals has been performed based on principal component analysis [70]. Based on an experimental dataset, the extracted features were employed as input to a deep neural network able to account for the variations due to different acquisitions temperatures. The outcomes of the architecture have been used to predict both probe position and defect geometrical characteristics (see Fig. 4.8). In [71], a 1D convolutional neural network has been designed in order to perform defect classification and regressions (i.e., defect height estimation) simultaneously based on a set of A-scan PECT experimental acquisitions. The obtained results have been compared with state-of-the-art machine learning algorithms (i.g., Gaussian process, support vector machine, decision tree, etc.) showed a great improvements obtained by the deep learning schema proposed. In the noteworthy work [72], Dang *et al.* authors proposed a deep neural network + involving CNN and long-short time memory architectures for characterizing the multiphase flow (e.g., oil and water percentage) for industrial applications showing the capability to accurately measure the volume fraction of water and the total flow velocity.

Deep neural network have also been applied to magnetic flux leakage (MFL) acquisitions in large pipeline loop, where artificial natural corrosion defects were present in a pipe [73, 74]. The dataset obtained from in-situ measurements has been

Figure 4.8 Deep neural network schema proposed in [70] to perform a regression task based on pulsed eddy current signals.

augmented by simulations based on rectangular shaped artificial defects. After that, both the datasets have been used for training a specific type of CNN, called visual transformation convolutional neural network (VT-CNN), for estimation of defect length, width and depth. The results obtained by the VT-CNN showed an higher accuracy compared to CNN without VT layer, provided a minor computational burden in training and testing phases. Sun *et al.* [75], proposed a physics-informed deep neural network architecture, called DfedResNet, to tackle the problem of estimation of defect(s) size parameters based on MFL acquisitions. The main features of such a deep CNN were the possibility of combining engineered features associated to MFL acquisitions (i.e., the physics-informed part [46, 47]) along with the spatial patterns of MFL images. Furthermore, saliency maps analysis has been also investigated for enhancing the interpretability of the deep learning schema proposed. The regression results obtained by the DfedResNet showed large improvements compared to support vector machine and VT-CNN schema. In [76] Le *et al.* proposed a convolutional neural network based surrogate model aiming at speeding up the computational time of magnetic field distribution based on the exploitation of finite element simulations. Toward this end, a U-Net like convolutional neural network was designed considering as input two images represented by the permeability and current distributions versus the magnetic field maps (x- and z- components). The results obtained showed the capability of the deep neural network architecture to accurately predict the numerical model test data in a wide set of scenarios (e.g., different flaw type, permeability values and current distributions).

4.4.2 Applications to the transportation and civil infrastructures sectors

Eddy current testing methods and techniques have been widely used in the past for detecting defects in aeronautic and aerospace industrial sectors thanks to the possibility to inspect rapidly (i.e., without needing to remove coating and/or fasteners) large airplane parts, fastener sites and bolt holes. Typically, corrosion like defects and micro cracks nearby fastener sites are the most critical defects to be detected in order to extend the operational life of airplanes without harming the residual life of the structure. The application of deep neural network in such industrial domain started in the beginning of this century. The use of two hidden layers feed forward neural network applied to defect classification based on PECT signals exploiting different feature engineering methods was studied in [50, 77]. Further studies on the use of ML algorithms for defect detection in multilayered metallic structures based on time domain (pulsed) ECT have been presented in [78] for detection of second-layer crack(s). More specifically, C-scan PECT data have been acquired on a structure composed by bolt hole with and without defect(s), bolt hole with counter sink with and without defect(s), hole with titanium and ferrous fastener with and without de-

fect(s). The detection performance of established machine learning algorithms such as random forest, gradient boosting and support vector machine have been assessed against deep learning methods based on long-shot term memory (LSTM) recurrent neural network (RNN) and multilayer perceptron (MLP) algorithms [45]. The results obtained showed that random forest and gradient boosting have an edge in performance compared to deep neural network methods once applied on raw PECT data. In [79], time harmonic ECT has been used to for defect classification based on experimental measurements in titanium plate based on tailored CNN network architecture dealing with the small amount experimental data available. The promising classification results obtained by the CNN architecture have been also compared with more established learning algorithms such as deep belief network, stacked autoencoder and support vector machine, showing that CNN was able to achieve the best results based on the test data.

The use of ECT method coupled with deep learning has been also proposed for detecting anomalies on railways in order to exploit the strength of ECT compared to visual inspection methods (e.g., robustness with respect to environmental conditions, high speed acquisitions, etc.). In [80], the alternating current field measuring technique has been used in order to perform experimental measurements on a calibration block containing clusters of cracks and a two hidden layers multilayer perceptron neural network have been used along a Bayesian regularization method for back-propagation schema. Simulations have been used to build the training set. The results obtained showed a good generalization capability on the studied DL schema in retrieving the equivalent length of the cluster of cracks on both simulated and experimental test sets. In [81], a data driven convolutional neural network architecture has been developed in order to exploit the ECT acquisitions post-processed through wavelet-based algorithms (i.e., continuous wavelet transform) and perform classification of surface breaking and superficial anomalies in rails (i.e., weld, squat and joint anomalies). The CNN architecture has been trained with data processed by wavelet power spectrum transform and the obtained classification results have been compared with a large set of classification methods involving logistic regression, ensemble methods, quadratic discriminant analysis, etc. The CNN results showed an edge in performance compared to the other ML methods studied.

In *et al.* [82], a Deep Belief Network (DBN) [45] composed by a set of stacked restricted Boltzman machines trained in an unsupervised fashion (i.e., see Fig. 4.9) has been applied in order to extract the most meaningful set of features from ECT signals measured on titan plates where slots and holes machined defects were embedded. The features extracted by DBN in an unsupervised way have been fed to vector valued Least Square Support Vector Machine (LS-SVM) algorithm in order to perform the defect characterization (i.e., defect(s) sizing) tasks. Thanks to the use of the DBN, the proposed method do not require any feature engineering stage before providing data to LS-SVM algorithms. The results obtained by the proposed learning schema have been compared with principal component analysis and Boltzman machine feature extraction algorithms. These comparisons showed that the higher accuracy was obtained by the DBN and LS-SVM approach. In [83], the use of two chained artificial neural network architectures has been developed in order to per-

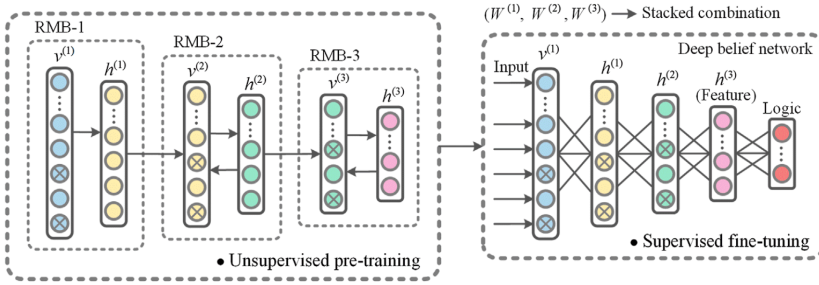

Figure 4.9 Deep belief network schema developed for unsupervised feature extraction based on ECT measurements in titanium plates [82] (CC BY 4.0 license).

form classification of defect depth and width based on MFL experimental measurements on steel wire ropes. The developed schema was based on the use of engineered features extracted from acquisitions. The obtained results showed the capability of the developed methodology to diagnose defects in wire ropes with good accuracy.

In civil infrastructures industrial sectors Ground Penetrating Radar (GPR) is widely applied to detect, classify and possibly localize buried objects under the soils or pavements, in reinforced concrete structures and masonry (e.g., landmines, pipes, voids, cracks, rebars). Deep convolutional neural network for detecting buried explosives based on GPR B-scans measurements has been proposed in [84]. The schema proposed is based on a pre-processing step aiming at detecting and selecting a suitable region of interest from the original B-scan before performing the training phase. The results obtained, compared with different the state-of-the-art algorithms for anomalies detection, showed that the CNN approach has the capability to outperform other traditional post-processing algorithms. In [85], experimental B-scan images have been decomposed into smaller patches containing buried landmine signatures (i.e., echos hyperbolas) and ground signatures before training a convolutional neural network targeting landmines detection. High detection accuracy in detecting landmine has been observed on the test set data for the three tested architectures compare to histogram oriented gradients detection procedure. In [86, 87, 88], different 3D convolutional neural network architectures have been developed in order to jointly use the information contents of B-, C- and D- scans GPR experimental acquisitions targeting objects detection. The results obtained showed an enhanced accuracy in classification results compared to classical approaches based on the use of B-scans only training input data. Automatic GPR signatures detection have been studied by several scholars for identify and classify echos hyperbolas in measured data. More into details, mask and faster Region-based Convolutional Neural Network (R-CNN) based architectures have been employed to detect hyperbolas performing semantic segmentation of echoes in B-scan measurements [89, 90, 91, 92, 93]. In [94, 95] different versions of YOLO architectures have been studied to tackle the hyperbolas identification and defect localization tasks based on B-scans acquisitions. A worthy mention on the use of deep learning methods applied to GPR data, is about the

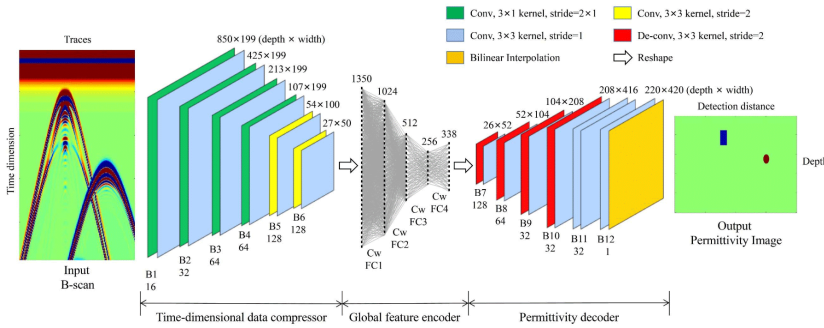

Figure 4.10 Convolutional neural network used for predicting ground permittivity characteristics based on GPR B-scan signals [98] (Copyright IEEE).

estimation of permittivity characteristics and electromagnetic waves velocity estimations in complex soils. Researchers are investigating the use of of deep generative models in order to perform a pixel-wise reconstruction of electromagnetic characteristic of soils based on encoder-decoder, U-Net like and generative adversarial network architectures [96]. Furthermore, tailored convolutional neural network architectures proposed in [97, 98, 99, 100] showed high capability in retrieving permittivity characteristics as well as velocity of electromagnetic in complex soils (i.e., see Fig. 4.10). It is worth to be mentioned that the previously cited works rely on simulated results for 2D problems only and that the performance of the DNN model developed is directly linked to the number of training samples considered, i.e., a large or very large training set is needed. Furthermore, a noteworthy result targeting forward and inverse modelling based on the use of deep fully connected neural network has been shown in [101, 102]. In these works Giannakis *et al.* employed DL schemas to infer rebars positions and size in concrete based on the use of fully numerical training sets.

4.4.3 Applications to the manufacturing and agri-food sectors

The Industry 4.0 paradigm, roughly consisting in global digitization and exploitation of data coming from manufacturing processes, for the next generation production and manufacturing plants aim at bringing the third industrial revolution in our society. This production paradigm is expected to extensively exploit the emerging technologies boosted by the most recent AI advances. In this regard, the wide use of robotics and numerically controlled procedures will be used for enhancing the production outcomes, lowering the production time and costs and increasing the production quality (i.e., the so-called zero-defects production). Toward this end, production chains are becoming more and more connected through a broad variety of possibly heterogeneous sensors aiming at collecting the largest set of information to control the productions factors (e.g., quality of manufactured specimens, devices, etc.). The integration, connection and exploitation of such heterogeneous set of information is among the highest challenges of AI-based algorithms for the next decade.

Microwave-based NDT&E method is applied in different manufacturing sectors for checking the quality of products during the fabrication process for dielectric of weakly conductive materials. In [103, 104], a convolutional neural network approach aims at retrieving the moisture density in porous foam inspected by a microwave tomography system. Toward this end, numerical simulations have been used in order to generate the training, validation and test sets. The real and imaginary parts of S-parameters have been fed to a CNN composed by two CNN blocks and a fully connected layer that, once reshaped, provided a vertical slice of the moisture density and/or the permittivity map(s). Microwave non-destructive testing and shallow neural networks have been jointly applied more than twenty years ago in the agri-food industrial sector [105] to establish the moisture content in wheat. More recently, [106] proposed a deep neural network architecture aiming at handling multi-frequency sweep microwaves measurements in order to predict the moisture measurement of sweet corn. A noteworthy end-to-end experimental set-up, exploiting both CPU or FPGA hardware, based on the use of microwaves and deep neural network learning schema has been developed for detecting contaminant in food jars [107]. Microwave inversion of dielectric rods in complex geometry in a fully data-driven approach exploiting convolutional neural network and recurrent neural network have been recently proposed by Ran *et al.* [108, 109] successfully comparing the obtained results with the state-of-the-art microwave imaging techniques. In [110], Wu *et al.* proposed a deep convolutional neural network architecture, called VMFNet (i.e., see 4.11), aiming at performing damage detection on curved radar absorbing materials (RAM). The designed network exploits the inputs coming from visual and microwave images of curved RAMs through two distinct backbone convolutional neural network, thus the extracted features have concatenated in order to perform detection. The results obtained by the proposed network showed large improvements in detecting cracks compared to state-of-the art algorithms in computer vision (e.g., YOLOv4, Faster R-CNN, EfficientNet). Rohkohl *et al.* [111] studied a deep learning schema aiming at perform weld inspection of electric contact in battery cell manufacturing based on eddy current testing. In particular, the authors proposed to train DNN model based on ECT signals in order to predict results from a reference method such as radiography testing in order to enhance the interpretation of ECT acquisitions. A convolutional neural network with U-Net like architectures has been developed in order to encode ECT into RT tomography map. Generated results based on the ECT tests are converted to cone beam tomography results that can be easily interpreted by humans without performing any expensive and time consuming ionizing RT tomography acquisitions.

Automatic characterization of magnetic properties and the design of innovative materials based on the used of machine learning are catching the interest of academic researchers and development engineers in the manufacturing industry. In [113], Elman neural network was used for the identification of non-linear hysteresis model parameters. More recently, in [114] a recurrent neural network model was used to accurately predict the behavior of the hysteresis loops in ferromagnetic materials under a limited amount of measurement data available. In Maciusowicz *et al.* [115], magnetic Barkhausen noise measurements have been exploited in order to predict grain

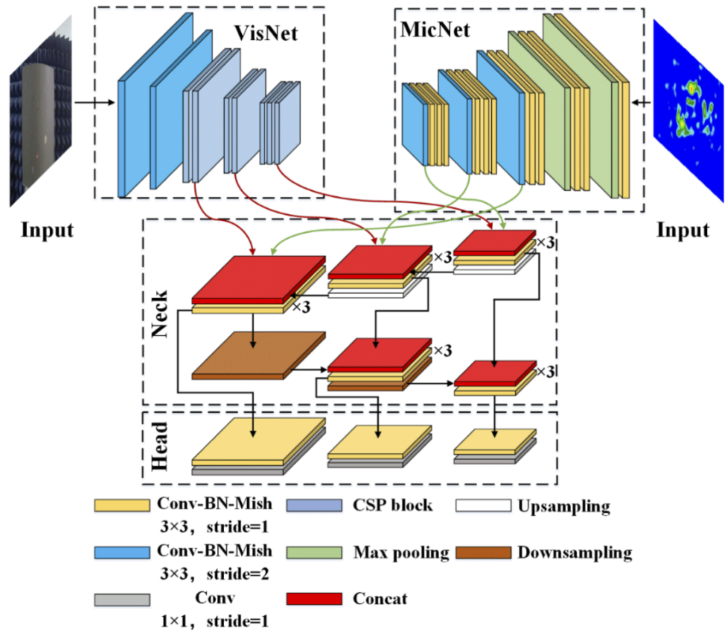

Figure 4.11 *Deep convolutional neural network applied to defect detection in radar absorbing materials based on visual and microwave features exploitation [110]. (CC BY 4.0 license)*

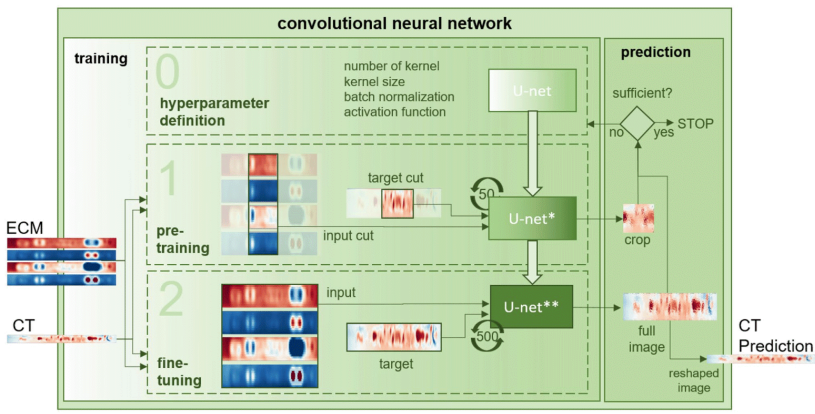

Figure 4.12 *Deep learning schema used to enhanced the interpretation of Eddy Current Measurements (ECM) based on the use of X-ray Computer Tomography (CT) data [111, 112] (CC BY 4.0 license).*

orientation in a ferrosilicon alloy for electrical steel. More into details, short-time Fourier transform has been applied on magnetic Barkhausen noise measurements, then the obtained signal maps have been fed to a specifically designed convolutional neural network. The obtained results showed the possibility to correctly classify the grains orientation angles for the experimental set-up considered.

4.5 Applications to higher frequency NDT&E methods

Accordingly to the schema displayed in Fig. 4.2, the highest frequencies of the electromagnetic spectrum are taken by three widely used NDT&E methods: Infrared Thermography Testing (ITT), Terahertz waves Testing (TT) and Radiography Testing (RT). Compared to lower-frequency methods, the interaction phenomena between source and inspected media is very different from low-frequency electromagnetic-based NDT&E method. ITT, TT and RT measurements are widely used methods along with electromagnetic NDT&E such as ECT or MFL testing. It is believed that this section can provide some alternative point of views of deep learning in NDT&E and suggest possible data hybridization and fusion across the different NDT&E methods treated in this work. In the following we provide an overview on how deep learning is applied to ITT, TT and RT.

4.5.1 Infrared thermography testing and terahertz wave testing

Infrared thermography testing is a NDT&E method that exploits thermal signatures of the SUT interacting with a controllable external excitation thermal source (eddy current induction, lamp flash, laser, etc.). In ITT, the interactions between thermal source and SUT are ruled by the convection and conduction equations that make ITT a complementary method to ECT and MFL. Indeed, ITT is one among the best suited methods for fast inspection of composite material and surface breaking defects in conducting media, masonry and concrete structures [116].

The thermal signature emitted by the SUT is collected by infrared cameras and lenses sensing rays within the infrared spectrum. Depending on the considered problem, ITT collected signals behaves as order-1 tensor if pixel-wise time-dependent measurements are considered. Order-2 and order-3 tensors are considered when acquisitions behave as images or video sequences, respectively. In this framework, deep learning techniques issued from image and signal processing communities have been adapted to ITT data. In particular, for order-1 tensor data are exploited when a limited amount of data is available. In [117, 118, 119], temperature time series signals are analyzed employing recurrent neural networks, where the temperature signatures were processed by employing a long-short memory recurrent neural network (LSTM-RNN) to classify different defects that typically affect carbon fiber reinforced plastic (CFRP) material in assembled structures. In [120, 121], a data-drive approach has been used to train a 1D CNN architecture in order to perform pixel-wise pristine vs. damage classification of CFRP material based on temperature signature with respect to time. The prediction results were subsequently concatenated in order to obtain an binarized image of the whole specimen under testing.

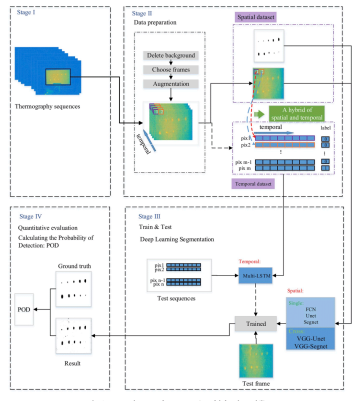

a)

Figure 4.13 Example of spatial and/or time feature based deep neural networks applied to ITT. A defect detection schema based an deep neural network architecture based on fully-connected network, VGG architecture and LSTM-RNN is displayed [123] (Copyright Elsevier).

The classification results have been compared with classic ITT signal processing state-of-the-art techniques showing promising improvements.

In Xie *et al.* [122], an autoencoder (AE) -based architecture has been studied in order to extract the meaningful set of hidden features associated to an experiment temperature time-series back-wall cracks; the proposed methodology showed to be able to enhance the quality of ITT images. Deep neural network architectures based on CNN and/or LSTM-RNN have been developed based on order-2 and order-3 tensor ITT inputs signals in order to gather and mix both spatial and temporal features [123, 124, 125] (i.e., see Fig. 4.13. Subsequently, the joint exploitation of both spatial and temporal features information allowed to increase the classification and regression performance compared to state-of-the art approaches. Deep neural network architecture has been also used in ITT to provide fast and reliable image segmentation [126, 127] to improve the image analysis stage. In [126], authors proposed a DNN architecture based on convolutional layers and Inception modules chained for tackling the problem of automatic segmentation of cracks profile in concrete structures. The inputs to the network are composed by hyper-spectral image gathering both visible and infrared spectra information the classification outputs obtained can be also interpreted in terms of probabilities being concrete or crack pixels.

The use of deep learning methods applied to ITT is also raising the interest of the experimental physics research community historically involved in numerical simulations of highly complex problems in a vast set of research domains. Very recently, the use of DL algorithms has been extensively used in order to model complex interactions between plasma and confinement barriers in fusion reactors. That is, ITT is used for in-service monitoring of plasma facing components to detect unexpected hot points to be handled instantaneously in order to avoid fusion reactor damages.

Simulated heat flux images have been used to predict plasma parameters based on a set of six different deep neural networks involving feed-forward neural network to deep Inception ResNet [128]. In [129], a generative adversarial network framework has been developed for enhancing the defect detection capabilities based on ITT measurements performed on composite fibre reinforced plastic plate. In [130], deep residual network have been used for deblurring purposes based on ITT image acquisitions.

Terahertz wave testing is used in NDT&E to perform contactless measurements of millimiter an submillimeter electromagnetic waves interacting with the SUT. The use of TT is gaining particular attention in NDT&E research community for inspecting dielectric materials such as glass fiber reinforced plastic, glass fiber composite, ceramics, plastic materials and in food industry. In [131], Wang *et al.* proposed an experimental validation of two different deep learning architecture for pixel-wise defect depth classification. That is, a bidirectional LSTM-RNN and a 1D-CNN were fed with time-domain signals or spectral signals and the results obtained by the two different architectures as well as the different input signals have been compared showing an edge in performance by the 1D-CNN regarding the input signals considered. In Zhang *et al.* [132], time domain TT measurements have been used in order to perform air gap thickness measurements in insulation equipment. Different ML classification methods have been trained and tested and compared on the experimental signals. That is, the performance results have been studied based on a deep learning schema composed by a chain of combination of CNN, residual shrinkage network and fully connected blocks as backbone for Terahertz waveform feature extraction purpose with a classification block provided by a Bayes classifier, a softmax layer or a support vector machine. The best results were obtained by using the support vector machine layer. Very recently, the use of deep learning for super-resolution purposes based on terahertz imaging images is attracting the attention of many researchers in the NDT&E field. In particular, in [133, 131, 134] tailored deep convolutional neural network architectures have been proposed to enhance the resolution of Terahertz images based on measurements performed on different kind of structures. In [135, 136], the super-resolution task have been tackled by considering generative adversarial network adapted to a dataset of experimental Terahertz images.

4.5.2 Radiographic testing

X-rays are a form of electromagnetic radiation of extremely short wavelength, ranging from 10^{-12} to 10^{-8} meter, that have the ability to penetrate the matter. The inspection of the internal structure of an object through X-ray testing consists in passing an X-ray beam through this object and recording its attenuation on a receptor. With digital radiography, a 2D grey-level projection image is acquired from the transmitted X-ray beam. Due to the similarities between the X-ray images and the visual ones, all modern computer vision techniques have been naturally applied to X-ray testing [137]. In particular, DL approaches have been employed to target real-time detection and automatic classification of encountered flaws, contaminants or threats for different industrial applications such as quality control of welds, inspec-

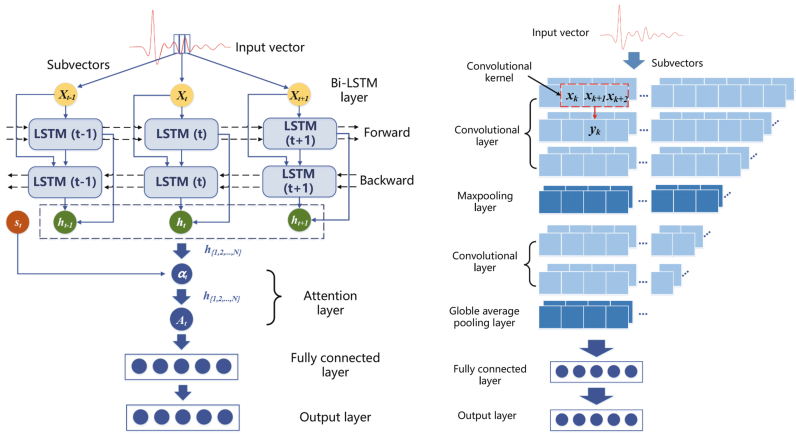

Figure 4.14 Deep neural network architecture as applied to Terahertz testing acquisitions. On the left a bidirectional LSTM-RNN and 1*D-CNN architecture are sketched, respectively [131] (Copyright Elsevier).*

tion of automotive and aeronautics parts, and food products or baggage screening. In this section, we present the most relevant applications of DL algorithms to RT data in different industrial sectors (defect detection in welds and casting parts, contaminants in food industry, threats in baggage screening).

Defects detection in weld inspection, casting and assembled parts

X-ray quality inspection of welds (e.g., pipes in NPP), casting light-alloy parts (e.g., wheel rims, steering knuckles and steering gear boxes) and assembled (e.g., composite structures) parts is commonly used in the nuclear, naval, chemical, automotive and aeronautical industries for ensuring the safety and the quality of the parts. Traditionally, radiographic images are manually inspected by human experts in order to detect and characterize potential defects. However, this task requires experienced inspectors and is time-consuming. In order to avoid the effect of human factors, to cope with the throughput of the production and analysis pipeline and to improve detection accuracy, fully automated inspection systems are deployed.

In the last decades, several works have focused on the automatic detection and identification of the most common welding defects and deep learning approaches have recently been applied to this task. In [138], the implementation of the automatic defect detection relies on three steps: the segmentation of the weld area, the application of a classification model on patches of the image and the detection of defects in the entire weld area using a sliding window algorithm. The classification model is constructed by stacking several sparse auto-encoders performing unsupervised learning and one softmax classifier using supervised learning. The proposed algorithm is applied on the public database GDXray [139] that includes a weld dataset of 88 images taken by the BAM Federal Institute for Materials Research and Testing. Several experiments are implemented including extracting the features using SAE and examining the classification accuracy under different parameters of

the model. The overall method is illustrated in Fig. 4.15. With this approach, defects can be accurately detected but not classified.

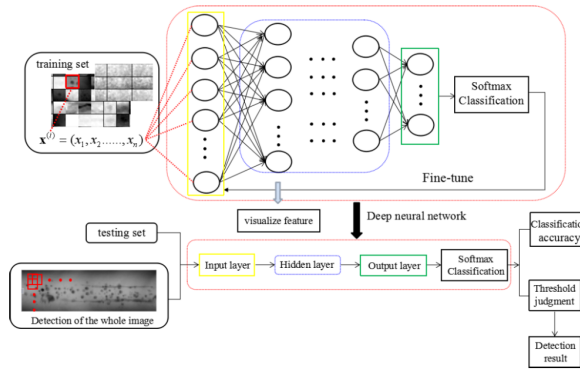

Figure 4.15 Illustration of the method proposed in [138] for defect detection in weld images (CC-BY 3.0 license).

Wang *et al.* [140] propose a method to identify three types of welding defects (blowhole, underfill or incomplete penetration) and their locations in X-ray images by using a pre-trained RetinaNet-based CNN and develop a dataset constituted of 6714 labelled images. Mean average precision (mAP) ratings are 0.76, 0.79, and 0.92 for the defect types. Yang *et al.* [141] proposed an improved CNN model based on LeNet-5, whose architecture consists of 7 layers (excluding the input layer), in which the layers 1, 3 and 5 are convolution layers, and the 2 and 4 are down-sampling layers. The CNN X-ray input is fed with 60×60 patches taken from the radiographic images and is shown to outperform LeNet-5, ANN, and SVM methods in terms of recognition accuracy.

Ferguson *et al.* [142] investigate the potential of different CNN architectures to localize casting defects in X-ray image. By decoupling the feature extraction layer from the object detection architecture, they studied three object detection architectures, namely Faster R-CNN, R-FCN (Region-based Fully Convolutional Networks [143]) and SSD (Single Shot Multibox Detector) with different feature extractors (VGG-16 and ResNet-101). Using an adapted version of the Faster R-CNN architecture, they achieve a mAP value of 0.921 on the GDXray dataset, constituted of 2727 X-ray images. For a similar use case, Du *et al.* [144] proposed Feature Pyramid Network (FPN) as the defect detection framework, which proved to be better suited for detecting small defects than Faster R-CNN, with a 40.9% improvement of the mAP. In the final regression and classification stage, RoIAlign (see Fig. 4.16) indicated apparent accuracy improvement in bounding boxes location compared with RoI pooling, which could increase accuracy by 23.6% under Faster R-CNN.

In general the proposed detection techniques cannot classify a lot of defect types with high accuracy, and do not consider the scale variation among different defect categories. Moreover, a lack of datasets, especially due to the lack of defective radio-

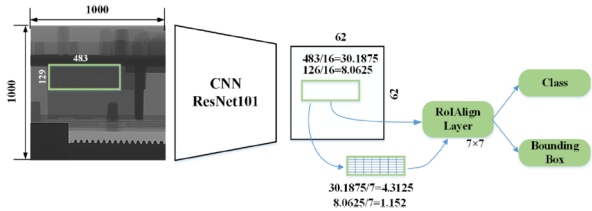

Figure 4.16 Faster R-CNN with RoIAlign applied to defect detection in X-ray images of casting parts [144] (Copyright Elsevier).

graphic images, is noted and justifies to investigate specific data augmentation techniques, transfer learning approaches and Generative Adversarial Networks (GAN).

Contaminants and threats detection in food industry and baggages

Ensuring contaminant-free products is a major concern in food industry, especially with the development of high-speed and fully automated production lines. X-ray inspection offers today the most effective way to detect and eliminate products containing foreign elements such as glass fragments, stones, metal pieces or organic external elements such as insects or wood chips. For the task of contaminants detection, unsupervised learning approaches could be preferred because they can learn only with contaminant-free images, much easier to record in industrial environment. However, because defective product images in the context of contaminant detection are only slightly different from legitimate ones, they cannot be well separated through one-class classification (OCC). For this reason, object class segmentation (OCS) is more commonly used for industrial flaw detection.

Bergmann *et al.* [145] propose a multi-object, multi-defect dataset of RGB camera images for anomaly detection and an evaluation of multiple OCS methods for unsupervised anomaly detection. Based on their results, Kim *et al.* [146] found OCS method not suitable for the contaminants detection in heterogeneous food items and proposed a supervised learning approach with a reduced dataset of industrial abnormal data. This database was augmented in a cut-paste manner using 500 images of different food product to create various backgrounds and fifty images of three types of contaminant without background (see Fig. 4.17). The test data were constructed from defective product X-ray images collected in the field. By predicting the test data with the object detection network YOLOv4 (see Fig. 4.18), trained on the augmented data, normal and defective products were classified with at least 94% accuracy for all foods.

Another use of industrial X-ray imaging concerns baggage screening, largely deployed for maintaining security at airports and other public spaces. In this field, screening is still very often realized by a human operator but due to the complexity of the image, containing lots of items overlapping, and the limited decision time, the performance of the control is not optimal. For this reason, several works have been dedicated to automatic threat detection. A thorough survey of this literature is reported in [147] based on 213 relevant references, among which 36 were identi-

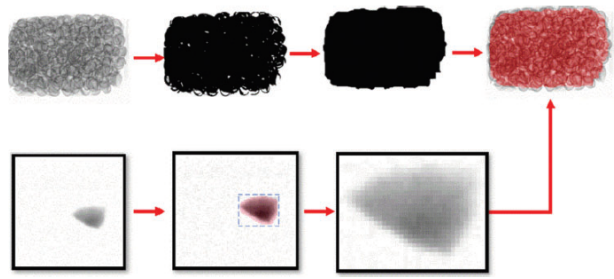

Figure 4.17 *Augmentation of the dataset by merging contaminants alone images in different backgrounds [146] (CC-BY 4.0 license).*

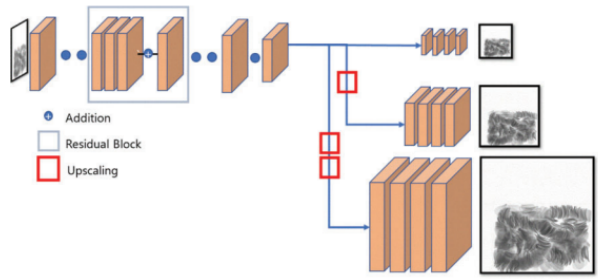

Figure 4.18 *Basic architecture of YOLOv3 applied to food package analysis in [146] (CC-BY 4.0 license).*

fied as using deep-learning algorithms and categorized as supervised (classification, detection and segmentation) and unsupervised (anomaly detection) approaches.

The performances of different supervised approaches, applied on a same input X-ray image, are illustrated in Fig. 4.19. For more details on the algorithms pipelines implemented in these different works, we refer the reader to [147].

Figure 4.19 *Results of DL tasks applied to X-ray baggage screening, the detection is performed with YOLOv5 on the GDXray dataset.*

Overall, despite promising results, the automated X-ray baggage screening remains an open question with a main limitation due to the lack of large unbiased datasets. There is also a lower detection accuracy in highly complex scenes and with thin objects such as sharps or knives with a critical role played here by multi-view X-ray systems, because there is a higher probability to have uninformative views

of the threat with such objects. However, modern X-ray detection systems provide two orthogonal views or even four different angles of the same object, potentially offering clearer perspectives of an object occluded in the first view. Here again, the datasets of multi-view X-ray imagery are scarce. Unsupervised anomaly detection approaches exhibit lower performances and could be improved.

4.6 Future trends and open issues for deep learning algorithms as applied to electromagnetic NDT&E

The broad survey performed in this chapter shed some light on the future trends in the application of DL algorithms in NDT&E. Active reach efforts are currently focused on hybridization of numerical solvers and deep learning algorithms, on the possibility to perform data fusion of NDT&E acquisitions for enhancing predictions accuracy, in the assessment and propagation of uncertainties in predictions, the interpretability and the explainability of deep learning decisions in the NDT&E.

Embedding the physics knowledge in deep learning architecture for electromagnetic NDT&E

The use of full data-driven approaches makes the deep learning methods behave like black-box models. In the context of NDT&E, the possibility to add either physical meaning or explainability to the DL model developed is an active field of study and research. Toward this end, the use of numerical solvers is envisaged in order to hybridize data-driven and physics-driven approaches or by conditioning the learning process by injecting the physics knowledge directly into the DL architecture [148, 149, 93, 150, 151, 152]. In both cases, the main goal is to end up with gray-box DL models that allow to better understand the (trained) models characteristics and discard unrealistic solutions from the physical point of view. Furthermore, the use of numerical solvers can be exploited to enhance the generalization capabilities of DL models when measurement data are subject to uncertainties.

Embedding explainability and interpretability in deep learning decision for electromagnetic NDT&E

The possibility to explain the ML models and the DL models specifically, also called explainable artificial intelligence (XAI), is a very active topic within the deep learning research community [153, 154, 155]. The XAI it will be one of the most active research field in NDT&E. Indeed, the possibility to link the prediction performed by the DL algorithms to the input features can lead, from the empirical point of view, to a better understanding and interpretation of the DL model mechanisms. In this framework, model-agnostic XAI algorithm are among the most suitable candidates [156, 157].

Quantify and propagate the uncertainties in deep learning based model for electromagnetic NDT&E

The application of DL to NDT&E acquisitions needs to account requirements in terms of prediction accuracy and robustness with respect to the test data provided

in the online phase. That is, the estimation of probabilities in predictions (e.g., classification classes) as well as the uncertainties associated to the predictions need to be considered [46, 47]. Bayesian inference applied to deep learning exploiting deep Bayesian Neural Network (BNN) architectures, can be used to estimate the DL model uncertainties also called epistemic uncertainties [66, 158]. The identification of the epistemic uncertainties enables as a consequence to estimate the aleatoric uncertainties linked to the intrinsic variability expressed by the measured data (e.g., measurement noise, uncertainties on probe position, probe ageing, specimen characteristics).

Data fusion based on deep learning algorithms applied to electromagnetic NDT&E

Deep learning methods are suitable to handle multiple structured input features during the learning process (e.g., multi-spectral images). In the context of electromagnetic NDT&E, such a feature allows, for instance, to handle directly complex valued signals in ECT. In the same manner researchers in NDT&E are trying to improve the prediction performances through the fusion of features coming from multiple channels data (e.g., multi-static probe signals, multiple frequencies). In wiev of deployment of DL algorithms in interconnected manufacturing systems, such a homogeneous data fusion process is supposed to be extended to non-electromagnetic NDT&E methods targeting an heterogeneous data fusion process. In this sense, a noteworthy result has been recently proposed in the biomedical context [159].

Open issues about the application of deep learning algorithms to electromagnetic NDT&E

It is well known that, in order to achieve good performance in terms of accuracy and robustness, DL algorithms need a suitable amount of data that often is larger than the one needed for other ML-based algorithms e.g., kernel machines. In NDT&E research community, due to secrecy and security issues, the availability of open dataset containing close-to-reality labelled data for developing and benchmark DL algorithms on a statistically meaningful set of samples is is very scarce. In fact, most of the available acquisitions have been performed on specimen that do not account realistic inspection set-up or defect typologies, thus the direct use of these datasets for training DL algorithms can be applied by the whole community on narrow and case dependent scenarios. Nevertheless, the joint use of numerical simulations and a small amount of labelled experimental data is believed to mitigate such systematic lack of realistic data through the use of semi-supervised and generative deep learning models.

Certification of NDT&E algorithms

Another great challenge to tackle in order to largely deploy such solutions in industry is the certification of DL based algorithms and their inclusions in the norms ruling its various sectors. Many aspects have indeed to be taken into considerations. First, the metrics used to compare performance between such diagnostic algorithms and existing procedures should be established, depending on the level of autonomy given to the algorithm: assistance of the operator to highlight suspect regions of the analyzed

data, proposition of diagnostic based on classification or fully automatic diagnostic. Then, when considering algorithms that update their learning with respect to incoming data, the question of how to ensure that the performance level is at least the same when adding some data should be answered to. Finally, another point is to manage the robustness of such algorithms (and possibly their recertification) to changes in the inspection conditions, like changes in environmental factors or replacement of parts of the acquisition chain due to some failures.

4.7 Conclusion and remarks

In this chapter, we analyzed some applications of deep learning methods to electromagnetic NDT&E and tried to show how deep neural networks can be adapted to different scenarios involving electromagnetic probing waves ranging from the quasi-static regime to microwave. In particular, CNN have been deeply exploited when the treated signals behave "as images" such as in the case of ECT and MFL inspections where real and imaginary parts of the impedance variation as well as the magnetic flux density are probed. Furthermore, time domain signals as in PECT or GPR measurements have been addressed, too, by employing LSTM-RNN and/or through CNN explicitly adapted for the purpose (e.g., pixel-wise inversion). Our analysis underlined that specifically tailored deep neural architectures have obtained a better prediction performances than pre-trained networks based on state-of-the-art architectures. In fact, the systematic lack of large shared datasets containing labelled measurements of realistic acquisitions make it difficult to properly benchmark and improve such backbone architectures. Moreover, the difficulties in collecting labelled measurements for defect parameters (e.g., the defect geometry) downsize the practical applications of deep learning models mostly to classification problems.

The survey performed in this chapter has also highlighted that the application of deep learning in NDT&E is also going toward the acceleration of numerical forward solvers for NDT&E modeling and simulations in a fully model-driven approach. It is believed that the ability of DL methods to handle problems having large cardinality (e.g., NDT&E parameters such as large number of defect classes, defect geometry description, etc.) will boost the research and its application to time consuming statistical studies (see, e.g., [160, 161]). Moreover, our analysis showed that the use of numerical solvers proves useful in designing the most suitable DL schemas as well as in improving the prediction accuracy when a low amount of measurements is available. Finally, a large amount of works in the literature showed that exploitation of deep learning algorithms directly on embedded systems (e.g., FPGA hardware) is already possible without an appreciable degradation in prediction performance.

4.8 Acknowledgements

The authors are grateful to Dominique Lesselier for all the wise advices, helpful suggestions and insightful comments concerning this manuscript. We deeply believe that this chapter improved a lot thanks to him.

References

[1] Marchand B, Decitre JM, Sergeeva-Chollet N, et al. Development of flexible array eddy current probes for complex geometries and inspection of magnetic parts using magnetic sensors. AIP Conference Proceedings. 2013;1511(1):488–493.

[2] Xie S, Chen Z, Takagi T, et al. Efficient numerical solver for simulation of pulsed eddy-current testing signals. IEEE Trans Magn. 2011;47(11):4582–4591.

[3] Xie S, Chen Z, Takagi T, et al. Development of a very fast simulator for pulsed eddy current testing signals of local wall thinning. NDT E Int. 2012;51:45–50.

[4] Xie S, Chen Z, Chen HE, et al. Sizing of wall thinning defects using pulsed eddy current testing signals based on a hybrid inverse analysis method. IEEE Trans Magn. 2013;49(5):1653–1656.

[5] Bowler JR, Johnson M. Pulsed eddy-current response to a conducting half-space. IEEE Trans Magn. 1997 May;33(3):2258–2264.

[6] Fu F, Bowler JR. Transient eddy-current driver pickup probe response due to a conductive plate. IEEE Trans Magn. 2006 Aug;42(8):2029–2037.

[7] Theodoulidis T. Developments in calculating the transient eddy-current response from a conductive plate. IEEE Trans Magn. 2008 Jul;44(7):1894–1896.

[8] Theodoulidis T, Skarlatos A. Efficient calculation of transient eddy current response from multilayer cylindrical conductive media. Phil Trans R Soc A. 2020;378:20190588.

[9] Skarlatos A, Theodoulidis T, Poulakis N. A fast and robust semi-analytical approach for the calculation of coil transient eddy-current response above planar specimens. IEEE Trans Magn. 2022 Sep;58(9):1–9.

[10] Dodd CV, Deeds WE. Analytical solutions to eddy current probe coil problems. J Appl Phys. 1968 May;39(6):2829–2838.

[11] Dodd CV, Cheng CC, Deeds WE. Induction coils coaxial with an arbitrary number of cylindrical conductors. J Appl Phys. 1974 Feb;45(2):638–647.

[12] Auld BA. Theoretical characterization and comparison of resonant-probe microwave eddy-current testing with conventional low-frequency eddy-current methods. In: George Birnbaum and George Free, Eds , American Society for Testing and Materials, editor. Eddy-Current Characterization of Material and Structures. vol. 12; 1981. p. 332–347.

[13] Auld BA, Muennemann F, Winslow DK. Eddy current probe response to open and closed surface flaws. J Nondestr Eval. 1981;2(1):1–21.

[14] Theodoulidis TP, Kriezis EE. Eddy Current Canonical Problems (with applications to nondestructive evaluation). Forsyth GA: Tech Science Press; 2006.

[15] Theodoulidis TP, Bowler JR. The Truncated Region Eigenfunction Expansion Method for the Solution of Boundary Value Problems in

Eddy Current Nondestructive Evaluation. AIP Conference Proceedings. 2005;760(1):403–408.

[16] Burke SK, Bowler JR, Theodoulidis TP. An Experimental and Theoretical Study of Eddy-Current End Effects In Finite Rods and Finite Length Holes. AIP Conference Proceedings. 2006;820(1):361–368.

[17] Bowler JR, Theodoulidis TP. Eddy currents induced in a conducting rod of finite length by a coaxial encircling coil. J Phys D: Appl Phys. 2005 Aug;38(16):2861–2868.

[18] Theodoulidis TP, Bowler JR. Eddy current coil interaction with a right-angled conductive wedge. Proc R Soc London, Ser A. 2005 Oct;461(2062):3123–3139.

[19] Theodoulidis TP, Bowler JR. Impedance of an induction coil at the opening of a borehole in a conductor. J Appl Phys. 2008 Jan;103(2):024905–1–024905–9.

[20] Skarlatos A, Theodoulidis T. Solution to the eddy-current induction problem in a conducting half-space with a vertical cylindrical borehole. Proc R Soc London, Ser A. 2012 Jun;468(2142):1758–1777.

[21] Skarlatos A, Theodoulidis T. Analytical treatment of eddy-current induction in a conducting half-space with a cylindrical hole parallel to the surface. IEEE Trans Magn. 2011 Nov;47(11):4592–4599.

[22] Skarlatos A, Theodoulidis T. Calculation of the eddy-current flow around a cylindrical through-hole in a finite-thickness plate. IEEE Trans Magn. 2015 Sep;51(9):6201507.

[23] Skarlatos A, Theodoulidis T. Impedance calculation of a bobbin coil in a conductive tube with eccentric walls. IEEE Trans Magn. 2010 Nov;46(11):3885–3892.

[24] Skarlatos A. A mixed spatial-spectral eddy-current formulation for pieces with one symmetry axis. IEEE Trans Magn. 2020 Sep;56(9):1–11.

[25] Chew WC. Waves and Fields in Inhomogeneous Media. New York: Wiley-IEEE Press; 1995.

[26] de Hoop AT. Handbook of Radiation and Scattering of Waves. Delft: Academic Press; 1995.

[27] Sabbagh HA. A model of eddy-current probes with ferrite cores. IEEE Trans Magn. 1987;23:1888–1904.

[28] Abubakar A, van den Berg PM. Iterative forward and inverse algorithms based on domain integral equations for three-dimensional electric and magnetic objects. J Comput Phys. 2004;195:236–262.

[29] Skarlatos A, Pichenot G, Lesselier D, et al. Electromagnetic modeling of a damaged ferromagnetic metal tube by a volume integral equation formulation. IEEE Trans Magn. 2008;44:623–632.

[30] Bowler JR. Eddy-current interaction with an ideal crack. I. The forward problem. J Appl Phys. 1994;75(12):8128–8137.

[31] Bowler JR. Eddy-current interaction with an ideal crack. II. The inverse problem. J Appl Phys. 1994;75(12):8138–8144.

[32] Bowler JR, Harfield N. Evaluation of probe impedance due to thin-skin eddy-current interaction with surface cracks. IEEE Trans Magn. 1998;34(2):515–523.

[33] Yoshida Y, Bowler JR. Thin-skin eddy-current interaction with semielliptical and epicyclic cracks. IEEE Trans Magn. 2000;36(1):281–291.

[34] Bowler JR, Harfield N. Vector potential integral formulation for eddy-current probe response to cracks. IEEE Trans Magn. 2000;36(2):461–469.

[35] Theodoulidis T. Developments in efficiently modelling eddy current testing of narrow cracks. NDT E Int. 2010;43(7):591–598.

[36] Theodoulidis T, Poulakis N, Dragogias A. Rapid computation of eddy current signals from narrow cracks. NDT E Int. 2010;43(1):13–19.

[37] Miorelli R, Reboud C, Theodoulidis T, et al. Efficient modeling of ECT signals for realistic cracks in layered half-space. IEEE Trans Magn. 2013 Jun;49(6):2886–2892.

[38] Bowler JR, Theodoulidis TP. Boundary element calculation of eddy currents in cylindrical structures containing cracks. IEEE Trans Magn. 2009;45:1012–1015.

[39] Pipis K, Skarlatos A, Theodoros T, et al. ECT-signal calculation of cracks near fastener holes using an integral equation formalism with dedicated Green's kernel. IEEE Trans Magn. 2016 Apr;52(4):6200608.

[40] Pipis K, Skarlatos A, Theodoulidis T, et al. Impedance of an Induction Coil Accounting for the End-Effect in Eddy-Current Inspection of Steam Generator Tubes. In: Noritaka Yusa HK Tetsuya Uchimoto, editor. Electromagnetic Nondestructive Evaluation (XIX). vol. 41 of Studies in Applied Electromagnetics and Mechanics. IOS Press; 2016. p. 237–244.

[41] Rebican M, Chen Z, Yusa N, et al. Investigation of numerical precision of 3-D RFECT signal simulations. IEEE Trans Magn. 2005;41:1968–1971.

[42] Chen Z, Rebican M, Miya K, et al. Three-dimensional simulation of remote field ECT using the Ar method and a new formula for signal calculation. Res Nondestr Eval. 2005;16:35–53.

[43] Miorelli R, Reboud C, Theodoulidis T, et al. Coupled approach VIM–BEM for efficient modeling of ECT signal due to narrow cracks and volumetric flaws in planar layered media. NDT E Int. 2014;62:178–183.

[44] Chen X, Wei Z, Li M, et al. A review of deep learning approaches for inverse scattering problems (invited review). Progress In Electromagnetics Research. 2020;167:67–81.

[45] Goodfellow I, Bengio Y, Courville A. Deep learning. MIT press; 2016.

[46] Hüllermeier E, Waegeman W. Aleatoric and epistemic uncertainty in machine learning: An introduction to concepts and methods. Machine Learning. 2021;110(3):457–506.

[47] Gawlikowski J, Tassi CRN, Ali M, et al. A survey of uncertainty in deep neural networks. arXiv preprint arXiv:210703342. 2021;.

[48] Coccorese E, Martone R, Morabito FC. A neural network approach for the solution of electric and magnetic inverse problems. IEEE transactions on magnetics. 1994;30(5):2829–2839.

[49] Elshafiey I, Udpa L, Udpa S. Application of neural networks to inverse problems in electromagnetics. IEEE transactions on magnetics. 1994;30(5):3629–3632.

[50] Lingvall F, Stepinski T. Automatic detecting and classifying defects during eddy current inspection of riveted lap-joints. NDT & E International. 2000;33(1):47–55.

[51] Chady T, Enokizono M, Sikora R. Neural network models of eddy current multi-frequency system for nondestructive testing. IEEE transactions on Magnetics. 2000;36(4):1724–1727.

[52] Chady T, Enokizono M, Sikora R, et al. Natural crack recognition using inverse neural model and multi-frequency eddy current method. IEEE transactions on Magnetics. 2001;37(4):2797–2799.

[53] Yusa N, Cheng W, Chen Z, et al. Generalized neural network approach to eddy current inversion for real cracks. NDT & E International. 2002;35(8):609–614.

[54] Wrzuszczak M, Wrzuszczak J. Eddy current flaw detection with neural network applications. Measurement. 2005;38(2):132–136.

[55] Chady T, Lopato P. Flaws identification using an approximation function and artificial neural networks. IEEE Transactions on Magnetics. 2007;43(4):1769–1772.

[56] Rosado LS, Janeiro FM, Ramos PM, et al. Defect characterization with eddy current testing using nonlinear-regression feature extraction and artificial neural networks. IEEE Transactions on Instrumentation and Measurement. 2013;62(5):1207–1214.

[57] Bilicz S, Lambert M, Gyimóthy S. Kriging-based generation of optimal databases as forward and inverse surrogate models. Inverse problems. 2010;26(7):074012.

[58] Douvenot R, Lambert M, Lesselier D. Adaptive metamodels for crack characterization in eddy-current testing. IEEE Transactions on Magnetics. 2011;47(4):746–755.

[59] Bernieri A, Betta G, Ferrigno L, et al. Multifrequency excitation and support vector machine regressor for ECT defect characterization. IEEE Transactions on Instrumentation and Measurement. 2013;63(5):1272–1280.

[60] Salucci M, Anselmi N, Oliveri G, et al. Real-time NDT-NDE through an innovative adaptive partial least squares SVR inversion approach. IEEE Transactions on Geoscience and Remote Sensing. 2016;54(11):6818–6832.

[61] Ahmed S, Reboud C, Lhuillier PE, et al. An adaptive sampling strategy for quasi real time crack characterization on eddy current testing signals. NDT & E International. 2019;103:154–165.

[62] Aldrin JC, Lindgren EA, Forsyth DS. Intelligence augmentation in nondestructive evaluation. In: AIP Conference Proceedings. vol. 2102. AIP Publishing LLC; 2019. p. 020028.

[63] EASA. Artificial Intelligence Roadmap - A human-centric approach to AI in aviation. EASA; 2020.

[64] EASA. First usable guidance for Level 1 machine learning applications. EASA; 2021.

[65] Cantero-Chinchilla S, Wilcox PD, Croxford AJ. Deep learning in automated ultrasonic NDE – developments, axioms and opportunities. 2021;.

[66] Zhu P, Cheng Y, Banerjee P, et al. A novel machine learning model for eddy current testing with uncertainty. NDT & E International. 2019;101:104–112.

[67] Park J, Han SJ, Munir N, et al. MRPC eddy current flaw classification in tubes using deep neural networks. Nuclear Engineering and Technology. 2019 Oct;51(7):1784–1790.

[68] Li S, Anees A, Zhong Y, et al. Crack Profile Reconstruction from Eddy Current Signals with an Encoder-Decoder Convolutional Neural Network. In: 2019 IEEE Asia-Pacific Microwave Conference (APMC); 2019. p. 96–98.

[69] Meng T, Tao Y, Chen Z, et al. Depth Evaluation for Metal Surface Defects by Eddy Current Testing Using Deep Residual Convolutional Neural Networks. IEEE Transactions on Instrumentation and Measurement. 2021;70:1–13.

[70] Buck JA, Underhill PR, Morelli JE, et al. Simultaneous Multiparameter Measurement in Pulsed Eddy Current Steam Generator Data Using Artificial Neural Networks. IEEE Transactions on Instrumentation and Measurement. 2016 Mar;65(3):672–679. Conference Name: IEEE Transactions on Instrumentation and Measurement.

[71] Fu X, Zhang C, Peng X, et al. Towards end-to-end pulsed eddy current classification and regression with CNN. In: 2019 IEEE International Instrumentation and Measurement Technology Conference (I2MTC); 2019. p. 1–5. ISSN: 2642-2077.

[72] Dang W, Gao Z, Hou L, et al. A novel deep learning framework for industrial multiphase flow characterization. IEEE Transactions on Industrial Informatics. 2019;15(11):5954–5962.

[73] Feng J, Li F, Lu S, et al. Injurious or noninjurious defect identification from MFL images in pipeline inspection using convolutional neural network. IEEE Transactions on Instrumentation and Measurement. 2017;66(7):1883–1892.

[74] Lu S, Feng J, Zhang H, et al. An estimation method of defect size from MFL image using visual transformation convolutional neural network. IEEE Transactions on Industrial Informatics. 2018;15(1):213–224.

[75] Sun H, Peng L, Huang S, et al. Development of a Physics-Informed Doubly Fed Cross-Residual Deep Neural Network for High-Precision Magnetic Flux Leakage Defect Size Estimation. IEEE Transactions on Industrial Informatics. 2022;18(3):1629–1640.

[76] Le M, Pham CT, Lee J. Deep neural network for simulation of magnetic flux leakage testing. Measurement. 2021 Jan;170:108726.

[77] Liu Z, Forsyth D, Lepine B, et al. Investigations on classifying pulsed eddy current signals with a neural network. Insight-Non-Destructive Testing and Condition Monitoring. 2003;45(9):608–614.

[78] Liu Y, Liu S, Liu H, et al. Pulsed eddy current data analysis for the characterization of the second-layer discontinuities. Journal of Nondestructive Evaluation. 2019;38(1):1–8.

[79] Deng W, Bao J, Ye B. Defect Image Recognition and Classification for Eddy Current Testing of Titanium Plate Based on Convolutional Neural Network. Complexity. 2020 Oct;2020:e8868190. Publisher: Hindawi.

[80] Rowshandel H, Nicholson G, Shen J, et al. Characterisation of clustered cracks using an ACFM sensor and application of an artificial neural network. NDT & E International. 2018;98:80–88.

[81] Alvarenga TA, Carvalho AL, Honorio LM, et al. Detection and Classification System for Rail Surface Defects Based on Eddy Current. Sensors. 2021 Jan;21(23):7937. Number: 23 Publisher: Multidisciplinary Digital Publishing Institute.

[82] Bao J, Ye B, Wang X, et al. A Deep Belief network and Least Squares Support Vector Machine Method for Quantitative Evaluation of Defects in Titanium Sheet Using Eddy Current Scan Image. Frontiers in Materials. 2020;7:322.

[83] Kim JW, Park S. Magnetic flux leakage sensing and artificial neural network pattern recognition-based automated damage detection and quantification for wire rope non-destructive evaluation. Sensors. 2018;18(1):109.

[84] Besaw LE, Stimac PJ. Deep convolutional neural networks for classifying GPR B-scans. In: Detection and Sensing of Mines, Explosive Objects, and Obscured Targets XX. vol. 9454. International Society for Optics and Photonics; 2015. p. 945413.

[85] Lameri S, Lombardi F, Bestagini P, et al. Landmine detection from GPR data using convolutional neural networks. In: 2017 25th European Signal Processing Conference (EUSIPCO). IEEE; 2017. p. 508–512.

[86] Kim N, Kim S, An YK, et al. Triplanar imaging of 3-D GPR data for deep-learning-based underground object detection. IEEE Journal of Selected Topics in Applied Earth Observations and Remote Sensing. 2019;12(11):4446–4456.

[87] Kang MS, Kim N, Lee JJ, et al. Deep learning-based automated underground cavity detection using three-dimensional ground penetrating radar. Structural Health Monitoring. 2020;19(1):173–185.

[88] Khudoyarov S, Kim N, Lee JJ. Three-dimensional convolutional neural network–based underground object classification using three-dimensional ground penetrating radar data. Structural Health Monitoring. 2020;19(6):1884–1893.

[89] Lei W, Hou F, Xi J, et al. Automatic hyperbola detection and fitting in GPR B-scan image. Automation in Construction. 2019;106:102839.

[90] Gao J, Yuan D, Tong Z, et al. Autonomous pavement distress detection using ground penetrating radar and region-based deep learning. Measurement. 2020;164:108077.

[91] Feng J, Yang L, Wang H, et al. GPR-based subsurface object detection and reconstruction using random motion and depthnet. In: 2020 IEEE Inter-

national Conference on Robotics and Automation (ICRA). IEEE; 2020. p. 7035–7041.

[92] Liu H, Lin C, Cui J, et al. Detection and localization of rebar in concrete by deep learning using ground penetrating radar. Automation in Construction. 2020;118:103279.

[93] Hou F, Lei W, Li S, et al. Improved Mask R-CNN with distance guided intersection over union for GPR signature detection and segmentation. Automation in Construction. 2021;121:103414.

[94] Li Y, Zhao Z, Luo Y, et al. Real-time pattern-recognition of GPR images with YOLO v3 implemented by Tensorflow. Sensors. 2020;20(22):6476.

[95] Li S, Gu X, Xu X, et al. Detection of concealed cracks from ground penetrating radar images based on deep learning algorithm. Construction and Building Materials. 2021;273:121949.

[96] Alvarez JK, Kodagoda S. Application of deep learning image-to-image transformation networks to GPR radargrams for sub-surface imaging in infrastructure monitoring. In: 2018 13th IEEE Conference on Industrial Electronics and Applications (ICIEA). IEEE; 2018. p. 611–616.

[97] Liu B, Ren Y, Liu H, et al. GPRInvNet: Deep Learning-Based Ground-Penetrating Radar Data Inversion for Tunnel Linings. IEEE Transactions on Geoscience and Remote Sensing. 2021;.

[98] Ji Y, Zhang F, Wang J, et al. Deep Neural Network-Based Permittivity Inversions for Ground Penetrating Radar Data. IEEE Sensors Journal. 2021;21(6):8172–8183.

[99] Leong ZX, Zhu T. Direct Velocity Inversion of Ground Penetrating Radar Data Using GPRNet. Journal of Geophysical Research: Solid Earth. 2021;p. e2020JB021047.

[100] Feng J, Yang L, Wang H, et al. Subsurface Pipes Detection Using DNN-based Back Projection on GPR Data. In: 2021 IEEE Winter Conference on Applications of Computer Vision (WACV). IEEE; 2021. p. 266–275.

[101] Giannakis I, Giannopoulos A, Warren C. A machine learning-based fast-forward solver for ground penetrating radar with application to full-waveform inversion. IEEE Transactions on Geoscience and Remote Sensing. 2019;57(7):4417–4426.

[102] Giannakis I, Giannopoulos A, Warren C. A machine learning scheme for estimating the diameter of reinforcing bars using ground penetrating radar. IEEE Geoscience and Remote Sensing Letters. 2020;18(3):461–465.

[103] Lähivaara T, Yadav R, Link G, et al. Estimation of moisture content distribution in porous foam using microwave tomography with neural networks. IEEE Transactions on Computational Imaging. 2020;6:1351–1361.

[104] Yadav R, Omrani A, Link G, et al. Microwave Tomography Using Neural Networks for Its Application in an Industrial Microwave Drying System. Sensors. 2021;21(20):6919.

[105] Bartley PG, Nelson SO, McClendon RW, et al. Determining moisture content of wheat with an artificial neural network from microwave transmission

measurements. IEEE Transactions on Instrumentation and Measurement. 1998;47(1):123–126.

[106] Zhang J, Du D, Bao Y, et al. Development of multifrequency-swept microwave sensing system for moisture measurement of sweet corn with deep neural network. IEEE Transactions on Instrumentation and Measurement. 2020;69(9):6446–6454.

[107] Ricci M, Štitić B, Urbinati L, et al. Machine-Learning-Based Microwave Sensing: A Case Study for the Food Industry. IEEE Journal on Emerging and Selected Topics in Circuits and Systems. 2021;11(3):503–514.

[108] Ran P, Qin Y, Lesselier D, et al. Subwavelength microstructure probing by binary-specialized methods: Contrast source and convolutional neural networks. IEEE Transactions on Antennas and Propagation. 2020;69(2):1030–1039.

[109] Ran P, Chen S, Serhir M, et al. Imaging of sub-wavelength microstructures by time reversal and neural networks, from synthetic to laboratory-controlled data. IEEE Transactions on Antennas and Propagation. 2021;69(12):8753–8762.

[110] Wu X, Wei X, Zhang L, et al. VMFNet: visual-microwave dual-modality real-time target detection model for detecting damage to curved radar absorbing materials. Optics Express. 2021;29(15):23182–23201.

[111] Rohkohl E, Kraken M, Schönemann M, et al. How to characterize a NDT method for weld inspection in battery cell manufacturing using deep learning. The International Journal of Advanced Manufacturing Technology. 2022;p. 1–15.

[112] Rohkohl E, Kraken M, Schönemann M, et al. How To Develop a NDT Method For Weld Inspection in Battery Cell Manufacturing Using Deep Learning. 18 June 2021;.

[113] Xu R, Zhou M. Elman neural network-based identification of Krasnosel'skii–Pokrovskii model for magnetic shape memory alloys actuator. IEEE Transactions on Magnetics. 2017;53(11):1–4.

[114] Grech C, Buzio M, Pentella M, et al. Dynamic Ferromagnetic Hysteresis Modelling Using a Preisach-Recurrent Neural Network Model. Materials. 2020;13(11):2561.

[115] Maciusowicz M, Psuj G, Kochmański P. Identification of Grain Oriented SiFe Steels Based on Imaging the Instantaneous Dynamics of Magnetic Barkhausen Noise Using Short-Time Fourier Transform and Deep Convolutional Neural Network. Materials. 2022;15(1):118.

[116] Vavilov V, Burleigh D. Infrared thermography and thermal nondestructive testing. Springer; 2020.

[117] Hu C, Duan Y, Liu S, et al. LSTM-RNN-based defect classification in honeycomb structures using infrared thermography. Infrared Physics & Technology. 2019 Nov;102:103032.

[118] Fang Q, Maldague X. A Method of Defect Depth Estimation for Simulated Infrared Thermography Data with Deep Learning. Applied Sciences. 2020

Jan;10(19):6819. Number: 19 Publisher: Multidisciplinary Digital Publishing Institute.

[119] Wang Q, Liu Q, Xia R, et al. Defect Depth Determination in Laser Infrared Thermography Based on LSTM-RNN. IEEE Access. 2020;8:153385–153393. Conference Name: IEEE Access.

[120] Cao Y, Dong Y, Cao Y, et al. Two-stream convolutional neural network for non-destructive subsurface defect detection via similarity comparison of lock-in thermography signals. NDT & E International. 2020;112:102246.

[121] Marani R, Palumbo D, Galietti U, et al. Deep learning for defect characterization in composite laminates inspected by step-heating thermography. Optics and Lasers in Engineering. 2021 Oct;145:106679.

[122] Xie J, Xu C, Chen G, et al. Improving visibility of rear surface cracks during inductive thermography of metal plates using Autoencoder. Infrared Physics & Technology. 2018;91:233–242.

[123] Luo Q, Gao B, Woo WL, et al. Temporal and spatial deep learning network for infrared thermal defect detection. NDT & E International. 2019;108:102164.

[124] Yang J, Wang W, Lin G, et al. Infrared Thermal Imaging-Based Crack Detection Using Deep Learning. IEEE Access. 2019;7:182060–182077.

[125] Müller D, Netzelmann U, Valeske B. Defect shape detection and defect reconstruction in active thermography by means of two-dimensional convolutional neural network as well as spatiotemporal convolutional LSTM network. Quantitative InfraRed Thermography Journal. 2020;p. 1–19.

[126] Jang K, Kim N, An YK. Deep learning–based autonomous concrete crack evaluation through hybrid image scanning. Structural Health Monitoring. 2019;18(5-6):1722–1737.

[127] Wu H, Zhang H, Hu G, et al. Deep learning-based reconstruction of the structure of heterogeneous composites from their temperature fields. AIP Advances. 2020 Apr;10(4):045037.

[128] Blatzheim M, Böckenhoff D, et al. Neural network regression approaches to reconstruct properties of magnetic configuration from Wendelstein 7-X modeled heat load patterns. Nuclear Fusion. 2019;59(12):126029.

[129] Liu K, Li Y, Yang J, et al. Generative principal component thermography for enhanced defect detection and analysis. IEEE Transactions on Instrumentation and Measurement. 2020;69(10):8261–8269.

[130] Jiang H, Chen F, Liu X, et al. Thermal wave image deblurring based on depth residual network. Infrared Physics & Technology. 2021;117:103847.

[131] Wang Q, Liu Q, Xia R, et al. Automatic defect prediction in glass fiber reinforced polymer based on THz-TDS signal analysis with neural networks. Infrared Physics & Technology. 2021;115:103673.

[132] Zhang Z, Peng G, Tan Y, et al. THz wave detection of gap defects based on convolutional neural network improved by residual shrinkage network. CSEE Journal of Power and Energy Systems. 2020;.

[133] Long Z, Wang T, You CW, et al. Terahertz image super-resolution based on a deep convolutional neural network. Applied Optics. 2019;58(10):2731–2735.

[134] Lei T, Tobin B, Liu Z, et al. A terahertz time-domain super-resolution imaging method using a local-pixel graph neural network for biological products. Analytica Chimica Acta. 2021;1181:338898.

[135] Lei T, Li Q, Sun DW. A Dual AE-GAN Guided THz Spectral Dehulling Model for Mapping Energy and Moisture Distribution on Sunflower Seed Kernels. Food Chemistry. 2021;p. 131971.

[136] Zhang Z, Zhang L, Chen X, et al. Modified Generative Adversarial Network for Super-Resolution of Terahertz Image. In: 2020 International Conference on Sensing, Measurement & Data Analytics in the era of Artificial Intelligence (ICSMD). IEEE; 2020. p. 602–605.

[137] Mery D. X-Ray Testing by Computer Vision. In: 2013 IEEE Conference on Computer Vision and Pattern Recognition Workshops; 2013. p. 360–367.

[138] Hou W, Wei Y, Guo J, et al. Automatic Detection of Welding Defects using Deep Neural Network. Journal of Physics: Conference Series. 2018 jan;933:012006.

[139] Mery D, Riffo V, Zscherpel U, et al. GDXray: The Database of X-ray Images for Nondestructive Testing. Journal of Nondestructive Evaluation. 2015;34.

[140] Wang Y, Shi F, Tong X. In: A Welding Defect Identification Approach in X-ray Images Based on Deep Convolutional Neural Networks; 2019. p. 53–64.

[141] Yang N, Niu H, Chen L, et al. X-ray weld image classification using improved convolutional neural network. vol. 1995; 2018. p. 020–035.

[142] Ferguson M, Ak R, Lee YTT, et al. Automatic localization of casting defects with convolutional neural networks. In: 2017 IEEE International Conference on Big Data (Big Data); 2017. p. 1726–1735.

[143] Dai J, Li Y, He K, et al. R-FCN: Object Detection via Region-Based Fully Convolutional Networks. In: Proceedings of the 30th International Conference on Neural Information Processing Systems. NIPS'16. Red Hook, NY, USA: Curran Associates Inc.; 2016. p. 379–387.

[144] Du W, Shen H, Fu J, et al. Approaches for improvement of the X-ray image defect detection of automobile casting aluminum parts based on deep learning. NDT & E International. 2019;107:102144.

[145] Bergmann P, Fauser M, Sattlegger D, et al. MVTec AD — A Comprehensive Real-World Dataset for Unsupervised Anomaly Detection. In: 2019 IEEE/CVF Conference on Computer Vision and Pattern Recognition (CVPR); 2019. p. 9584–9592.

[146] Kangjik K, Hyunbin K, Junchul C, et al. Real-Time Anomaly Detection in Packaged Food X-Ray Images Using Supervised Learning. Computers, Materials & Continua. 2021;67(2):2547–2568.

[147] Akcay S, Breckon T. Towards automatic threat detection: A survey of advances of deep learning within X-ray security imaging. Pattern Recognition. 2022;122:108245.

[148] Raissi M, Perdikaris P, Karniadakis GE. Physics-informed neural networks: A deep learning framework for solving forward and inverse problems involving nonlinear partial differential equations. Journal of Computational physics. 2019;378:686–707.

[149] Shukla K, Jagtap AD, Blackshire JL, et al. A Physics-Informed Neural Network for Quantifying the Microstructural Properties of Polycrystalline Nickel Using Ultrasound Data: A promising approach for solving inverse problems. IEEE Signal Processing Magazine. 2021;39(1):68–77.

[150] Guo R, Shan T, Song X, et al. Physics embedded deep neural network for solving volume integral equation: 2D case. IEEE Transactions on Antennas and Propagation. 2021;.

[151] Guo L, Li M, Xu S, et al. Electromagnetic Modeling Using an FDTD-Equivalent Recurrent Convolution Neural Network: Accurate Computing on a Deep Learning Framework. IEEE Antennas and Propagation Magazine. 2021;p. 2–11.

[152] Guo R, Lin Z, Shan T, et al. Physics embedded deep neural network for solving full-wave inverse scattering problems. IEEE Transactions on Antennas and Propagation. 2021;p. 1–1.

[153] Adadi A, Berrada M. Peeking inside the black-box: a survey on explainable artificial intelligence (XAI). IEEE access. 2018;6:52138–52160.

[154] Gunning D, Aha D. DARPA's Explainable Artificial Intelligence (XAI) Program. AI Magazine. 2019 Jun;40(2):44–58.

[155] Arrieta AB, Díaz-Rodríguez N, Del Ser J, et al. Explainable Artificial Intelligence (XAI): Concepts, taxonomies, opportunities and challenges toward responsible AI. Information fusion. 2020;58:82–115.

[156] Ribeiro MT, Singh S, Guestrin C. " Why should i trust you?" Explaining the predictions of any classifier. In: Proceedings of the 22nd ACM SIGKDD international conference on knowledge discovery and data mining; 2016. p. 1135–1144.

[157] Lundberg SM, Lee SI. A unified approach to interpreting model predictions. Advances in neural information processing systems. 2017;30.

[158] Wei Z, Chen X. Uncertainty quantification in inverse scattering problems with Bayesian convolutional neural networks. IEEE Transactions on Antennas and Propagation. 2020;69(6):3409–3418.

[159] Qin Y, Ran P, Rodet T, et al. Breast imaging by convolutional neural networks from joint microwave and ultrasonic data. IEEE Transactions on Antennas and Propagation. 2022;p. 1–1.

[160] Aldrin JC, Oneida EK, Shell EB, et al. Model-based probe state estimation and crack inverse methods addressing eddy current probe variability. In: AIP Conference Proceedings. vol. 1806. AIP Publishing LLC; 2017. p. 110013.

[161] Cai C, Miorelli R, Lambert M, et al. Metamodel-based Markov-Chain-Monte-Carlo parameter inversion applied in eddy current flaw characterization. NDT E Int. 2018;99:13–22.